BIOCHEMISTRY

ITIH4 acts as a protease inhibitor by a novel inhibitory mechanism

Rasmus Pihl[1], Rasmus K. Jensen[2], Emil C. Poulsen[2], Lisbeth Jensen[1], Annette G. Hansen[1], Ida B. Thøgersen[2], József Dobó[3], Péter Gál[3], Gregers R. Andersen[2], Jan J. Enghild[2], Steffen Thiel[1]*

Inter-α-inhibitor heavy chain 4 (ITIH4) is a poorly characterized plasma protein that is proteolytically processed in multiple pathological conditions. However, no biological function of ITIH4 has been identified. Here, we show that ITIH4 is cleaved by several human proteases within a protease-susceptible region, enabling ITIH4 to function as a protease inhibitor. This is exemplified by its inhibition of mannan-binding lectin–associated serine protease-1 (MASP-1), MASP-2, and plasma kallikrein, which are key proteases for intravascular host defense. Mechanistically, ITIH4 acts as bait that, upon cleavage, forms a noncovalent, inhibitory complex with the executing protease that depends on the ITIH4 von Willebrand factor A domain. ITIH4 inhibits the MASPs by sterically preventing larger protein substrates from accessing their active sites, which remain accessible and fully functional toward small substrates. Thus, we demonstrate that ITIH4 functions as a protease inhibitor by a previously undescribed inhibitory mechanism.

INTRODUCTION

Inter-α-inhibitor heavy chain 4 (ITIH4) is a liver-produced plasma protein belonging to the inter–α-inhibitor/ITIH family of proteins that consists of bikunin and six different heavy chain proteins (*1*). This protein family is also referred to as inter–α-trypsin inhibitor proteins since bikunin displays a weak inhibitory effect on proteases for which a biological role is yet to be defined (*2*, *3*). Bikunin and the ITIHs form covalent proteoglycan complexes that are involved in extracellular matrix remodeling and stabilization (*2*). While all ITIHs share similar N-terminal domain structures that include a von Willebrand factor type A domain (VWF), ITIH4 has a unique C-terminal region that contains a proline-rich region (PRR) (*4*) and a tectonin-like β-propeller repeat (*1*). ITIH4 lacks a C-terminal consensus sequence, which is present in all other ITIHs, that is required for the formation of bikunin-ITIH complexes. Consequently, ITIH4 is not incorporated into proteoglycan complexes and presumably functions independently of the other protein family members (*1*, *5*). ITIH4 is a poorly characterized protein, although it is relatively abundant with reported serum concentrations between 80 and 300 μg/ml (*5*). Generation of *itih4*$^{-/-}$ mice did not reveal any apparent phenotype besides some suppressed interleukin-6/signal transducer and activator of transcription 3 signaling (*6*). Plasma kallikrein has been shown to cleave ITIH4 within the PRR in vitro, which might result in the release of a bioactive peptide, analogous to the kallikrein-mediated release of bradykinin from high-molecular-weight kininogen (HMWK) (*5*). ITIH4 is fragmented within the PRR in cancer patients (*7*), in amyotrophic lateral sclerosis patients (*8*), in women experiencing recurrent pregnancy loss (*9*), and during chronic *Mycobacterium tuberculosis* infection (*10*). Nonetheless, the mechanisms and ramifications of ITIH4 cleavage are unknown, and the biological role of ITIH4 has remained unknown despite the accumulating evidence that links ITIH4 to human disease. In the present study, we uncovered a connection between ITIH4 and proteolytic enzymes, which is illustrated in detail by its interaction with plasma kallikrein and the mannan-binding lectin (MBL)–associated serine proteases (MASPs) from the lectin pathway (LP) of complement.

The complement system is an integral part of the innate immune system that is driven by consecutive proteolytic events. Complement can be activated through three routes: the LP, the classical pathway (CP), and the alternative pathway (AP), which all converge at the formation of enzymatic complexes called C3 convertases that cleave the protein complement component C3. Cleavage of C3 into C3a and C3b initiates downstream effector mechanisms of complement that include opsonization of the target surface, generation of proinflammatory mediators, and direct cell killing (*11*). The LP and CP are initiated by binding of pattern recognition molecules (PRMs) to repetitive molecular patterns on the surface of pathogens or altered self-surfaces. By contrast, the AP is constitutively active because of spontaneous activation of C3 in the fluid phase. The LP contains at least five carbohydrate-binding PRMs, of which the best characterized is MBL (also known as mannose-binding lectin), while H-ficolin (also known as ficolin-3) is the most abundant in humans (*12*). The PRMs are all able to associate with the homodimeric proteases MASP-1, MASP-2, and MASP-3. MASP-1 and MASP-2 circulate as zymogens that are activated when PRM-MASP complexes cluster on a surface. Subsequently, MASP-2 cleaves complement factor C4, while MASP-1 and MASP-2 both cleave C2, generating the C3 convertase C4b2a (*13*). MASP-3 contributes to the AP rather than the LP by converting zymogenic pro-factor D into active factor D (*14*, *15*), thereby facilitating C3 convertase formation.

The MASPs have similar domain architectures, and all consist of six domains (CUB1-EGF-CUB2-CCP1-CCP2-SP). The three N-terminal domains are responsible for MASP homodimerization and PRM binding; the CCP domains may influence the enzymatic properties of the proteases, whereas the SP domain constitutes the proteolytic entity (*16*). While MASP-2 and MASP-3 only have few substrates, MASP-1 is a promiscuous protease that propagates LP activation into a wide-ranging intravascular response (*17*). To prevent autoimmune injury, the proteolytic activities of MASP-1 and MASP-2 are tightly regulated, as is the case for most proteases. In general, the network and interrelationship between extracellular

[1]Department of Biomedicine, Aarhus University, Aarhus, Denmark. [2]Department of Molecular Biology and Genetics, Aarhus University, Aarhus, Denmark. [3]Institute of Enzymology, Research Centre for Natural Sciences, Budapest, Hungary.
*Corresponding author. Email: st@biomed.au.dk

proteases and their inhibitors are redundant and complex, as most proteases are inhibited by several inhibitors and most inhibitors have several proteolytic targets (*18*). Concordantly, MASP-1 and MASP-2 are inhibited by multiple inhibitors with numerous targets, including the suicide inhibitor C1 inhibitor (C1inh; also known as serpin G1) (*19*), antithrombin (also known as serpin C1) (*20*), and α-2-macroglobulin (α_2M) (*21*).

The multifaceted nature of MASP-1 prompted us to search for previously unidentified MASP-1 inhibitors or interactors, and we found that MASP-1 forms a stable complex with an 80-kDa fragment of the 120-kDa ITIH4. Furthermore, ITIH4 was shown to form similar complexes with MASP-2 and plasma kallikrein. This complex formation leads to protease inhibition by physically preventing cleavage of larger substrates, although the catalytic sites of the proteases remain active. Formation of noncovalent ITIH4-protease complexes was dependent on binding of a divalent cation by the VWF domain of ITIH4, which induces a global conformational change in ITIH4 that enables complex formation. ITIH4 is thus shown to inhibit proteases by a novel mechanism. We find that a number of proteases cleave ITIH4 in vitro, and their cleavage sites define a protease-susceptible region (PSR) within ITIH4, suggesting that ITIH4 may serve as a general protease inhibitor that targets multiple proteases.

RESULTS

ITIH4 forms complexes with the proteases MASP-1 and MASP-2 but not MASP-3

In the search of previously unknown MASP-1–interacting proteins, we simulated LP activation by adding an activated, catalytic fragment of MASP-1 consisting of the CCP1-CCP2-SP domains (MASP-1cf) to normal human serum. Subsequently, immunoprecipitation (IP) of MASP-1 was performed, and the sample was analyzed by SDS–polyacrylamide gel electrophoresis (SDS-PAGE) together with a control sample without addition of MASP-1cf (Fig. 1A). MASP-1cf–dependent bands were analyzed by liquid chromatography–tandem mass spectrometry (LC-MS/MS) to identify potential MASP-1 interactors (table S1). As expected, the majority of MASP-1 reacted with known inhibitors such as α_2M, C1inh, and antithrombin (*20*). Furthermore, the LP PRMs MBL, H-ficolin, and L-ficolin were identified because of pull-down of endogenous MASP-1 and MASP-3 (table S1). ITIH4 was identified in several bands and was particularly abundant in 80-kDa bands in both the reduced and nonreduced sample (Fig. 1, A and B).

To verify the interaction between MASP-1 and ITIH4 and to investigate whether all MASPs are able to bind ITIH4, we performed similar co-IP experiments using MASP-1cf, an activated CCP1-CCP2-SP fragment of MASP-2 (MASP-2cf), and a novel construct of activated, full-length MASP-3 K448Q. The K448Q mutation allows MASP-3 to be activated by C1r, yielding MASP-3 K448Q that was >90% activated and readily cleaved its biological substrate pro-factor D into factor D (fig. S1). Following anti-MASP IPs, anti-ITIH4 Western blotting (WB) showed that both MASP-1 and MASP-2 bound ITIH4 in serum (Fig. 1C). MASP-1 and MASP-2 copurified with an 80-kDa ITIH4 fragment, while a 60-kDa ITIH4 band was also seen for MASP-1. The ITIH4 bands were MASP1/2cf-dependent and were absent in isotype control IPs. By contrast, MASP-3 K448Q was not capable of binding ITIH4 (Fig. 1C). These samples were also used for anti-MASP WB, confirming that all IPs efficiently precipitated the respective MASP (Fig. 1, D to F). Noticeably, anti–MASP-1 WB resulted in a complex band pattern due to the generation of various covalent inhibitor–MASP-1 complexes (Fig. 1D). The formation of ITIH4–MASP-1/2 complexes was additionally verified using anti-ITIH4 IPs followed by anti-MASP WBs. Again, MASP-1cf and ITIH4 coprecipitated, as evidenced by a 27-kDa band corresponding to the SP domain of MASP-1 (Fig. 1G). Similarly, a 15-kDa CCP1-CCP2 MASP-2 band copurified with ITIH4 (Fig. 1H), whereas no ITIH4 binding was observed for MASP-3 K448Q (Fig. 1I). No MASP bands were identified in the absence of activated MASPs or using isotype control IPs (Fig. 1, G to I). Overall, these experiments demonstrate that MASP-1 and MASP-2 form complexes with fragments of ITIH4 in human serum.

Various proteases cleave ITIH4 within a PSR

Although intact ITIH4 migrates as a 120-kDa protein in SDS-PAGE, the ITIH4 that copurified with MASP-1/2 was generally identified at 80 kDa (Fig. 1, A and C). Moreover, fragmentation of ITIH4 was observed in serum upon incubation with MASP-1cf and MASP-2cf but not MASP-3 K448Q (fig. S2, A to C), suggesting that MASPs that bind ITIH4 also cleave it. To examine whether MASP-1 and MASP-2 cleave ITIH4 directly, recombinant ITIH4 was purified (fig. S2D) and incubated with the activated MASPs. MASP-1cf was found to cleave ITIH4 into 80- and 42-kDa fragments, and the 42-kDa fragment was further processed into a 37-kDa fragment (Fig. 2A). MASP-2cf cleaved ITIH4 slightly faster than MASP-1cf, producing an 85-kDa fragment, which was, subsequently, processed into an 80-kDa fragment and a 37-kDa fragment. All full-length ITIH4 was practically cleaved after 2 hours for both MASP-1 and MASP-2. Upon 24 hours of incubation, MASP-1 and MASP-2 both generated a 60-kDa fragment, indicating that this fragment was produced by secondary cleavage of the 80-kDa fragment (Fig. 2A). Thus, MASP-1 and MASP-2 generated ITIH4 fragments that corresponded in size to those fragments that copurified with the MASPs (Fig. 1). By contrast, MASP-3 K448Q was not capable of cleaving ITIH4, thereby reflecting its inability to bind ITIH4 (Fig. 2A). The cleavage sites of MASP-1 and MASP-2 in ITIH4 were mapped using N-terminal sequencing, which identified the cleavage sites as ^{644}RR^{645} and ^{688}RR^{689} /^{689}RL^{690} (Fig. 2B). MASP-1 initially cleaved within the ^{644}RR^{645} site and, subsequently, converted the 42-kDa fragment into a 37-kDa fragment by cleaving at the ^{688}RR^{689} site. The initial cut by MASP-2 occurred in the ^{689}RL^{690} site followed by cleavage within or in the vicinity of the ^{644}RR^{645} site.

We next asked whether the ability to cleave ITIH4 is widespread among proteases. In addition to the MASPs, we incubated ITIH4 with 15 different serine, metallo-, or cysteine proteases belonging to various biological systems and followed cleavage by SDS-PAGE (Fig. 2C and fig. S3, A to R). Eight of the proteases readily cleaved ITIH4 and had cleaved the majority of ITIH4 after 24 hours. In particular, MASP-2 and matrix metalloproteinase-7 (MMP-7) efficiently cleaved ITIH4, while robust cleavage was also observed for MASP-1, MMP-13, thrombin, papain, plasmin, and kallikrein. In addition, five proteases cleaved ITIH4 slowly and only displayed visible degradation after 24 hours, while four proteases did not cleave ITIH4 at all (Fig. 2C and fig. S3, A to R). To identify the cleavage sites for the initial cut (or cuts), we performed N-terminal sequencing on the protease-generated ITIH4 fragments. The cleavage site of kallikrein was identified to be ^{688}RR^{689}, as previously reported (*5*). In addition, a number of different cleavage sites that all clustered within the PRR of ITIH4 were identified for the human proteases (Fig. 2C and fig. S3S). Thus, we suggest that the PRR is instead referred to as the PSR

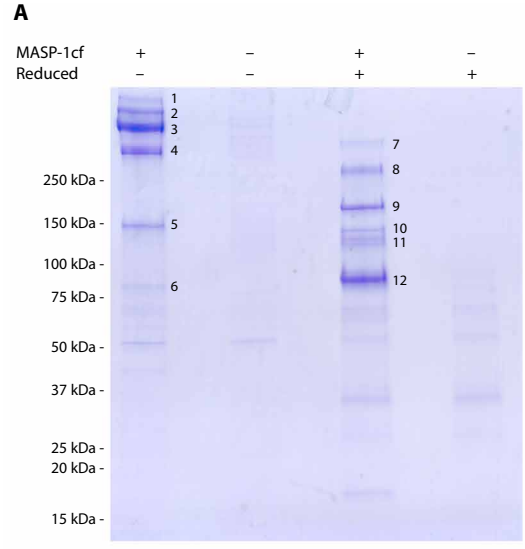

B

Band #	Protein ID	Score	Matches	Sequences
1	α_2M	2360	103	29
1	**ITIH4**	157	8	7
1	MASP-1	125	6	4
5	C1inh	1457	79	15
5	MASP-1	980	59	8
5	α_2M	757	26	15
5	**ITIH4**	123	3	3
5	H-ficolin	122	5	4
5	Plasma serine protease inhibitor	101	3	3
6	**ITIH4**	304	14	9
6	α_2M	124	3	3
11	α_2M	3596	158	29
11	MASP-1	736	47	9
11	C1inh	608	36	13
11	C3	148	6	6
11	ITIH4	138	5	5
12	α_2M	7804	312	42
12	**ITIH4**	2293	80	19
12	Antithrombin	465	19	8
12	MASP-1	328	15	7
12	Plasma serine protease inhibitor	139	4	4
12	Prothrombin	102	4	4

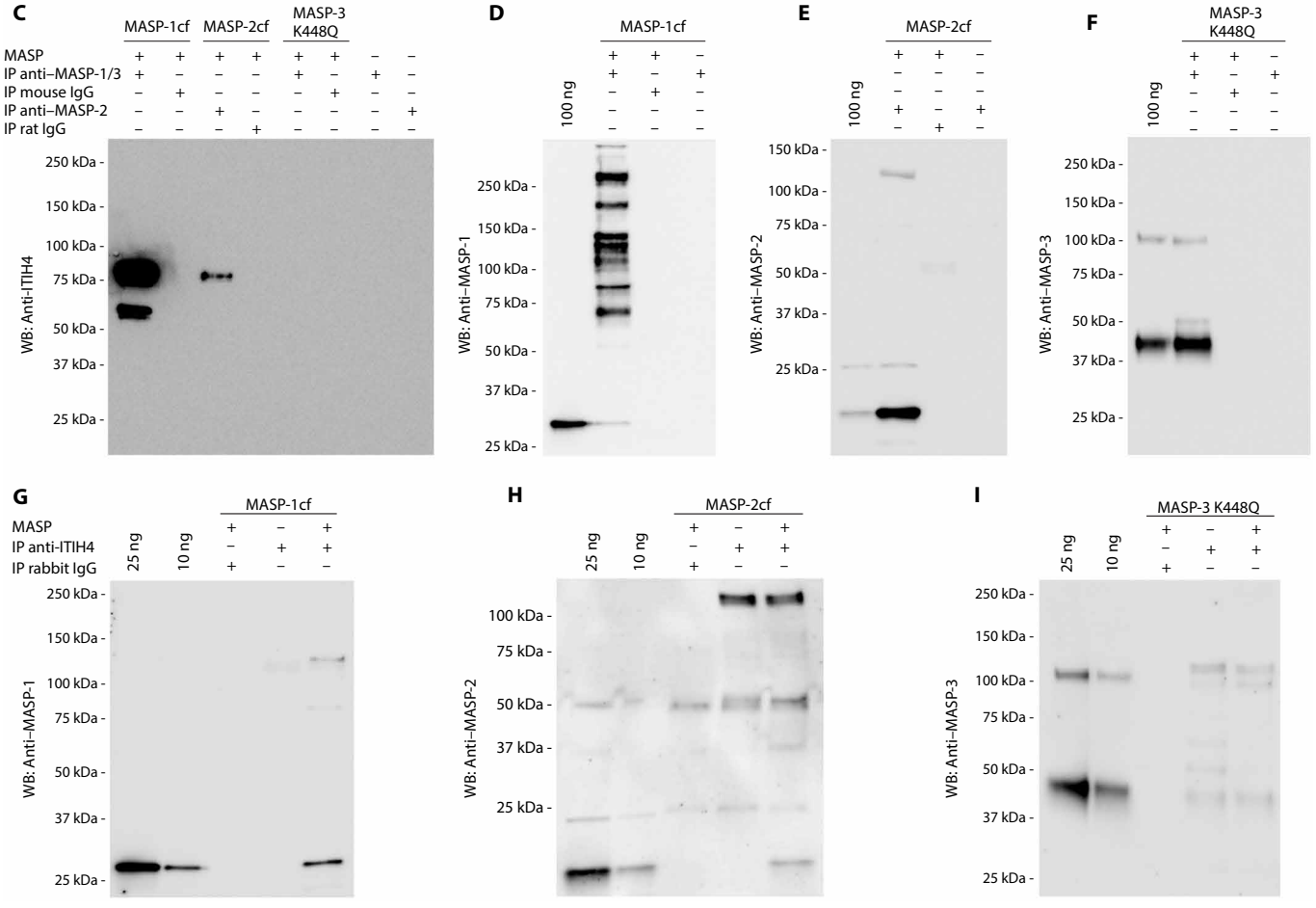

Fig. 1. ITIH4 coimmunoprecipitates with MASP-1 and MASP-2. In all experiments, activated MASPs were added to human serum followed by IP. (**A**) Reducing and nonreducing SDS-PAGE analysis of samples with or without MASP-1 addition. Numbers denote bands that were analyzed by LC-MS/MS. (**B**) LC-MS/MS analysis of ITIH4-containing bands. Band # refers to (A), and proteins are listed together with their Mascot protein score, number of peptides matching the protein, and the number of unique sequences that match the protein. The table only includes hits with a score >100 and >2 unique sequences. (**C**) IPs were performed using anti-MASP antibodies or isotype controls followed by anti-ITIH4 WB. Negative controls without addition of exogenous MASP were included. (**D** to **F**) The appropriate samples from (C) were analyzed using anti–MASP-1 WB (D), anti–MASP-2 WB (E), or anti–MASP-3 WB (F) together with 100 ng of the respective MASP. (**G** to **I**) WB analysis of anti-ITIH4 immunoprecipitated samples and 25 and 10 ng of the appropriate MASP. In each panel, the blot is developed with anti–MASP-1 (G), anti–MASP-2 (H), or anti–MASP-3 (I). All blots in this figure are representative of three repeated experiments. IgG, immunoglobulin G.

A

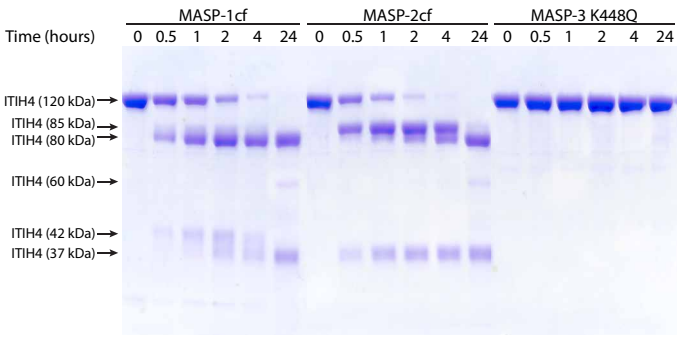

B

	N terminus generated by	
ITIH4 fragments	**MASP-1cf**	**MASP-2cf**
120 kDa (FL)	^{28}EKNGIXIYSL	^{28}EKNGIXIYSL
85 kDa	^{28}EKNGIDIYSL	^{28}EKNGIDIYSL
80 kDa	^{28}EKNGIDIYSL	^{28}EKNGIDIYSL
60 kDa	^{28}EKNGIDIYSL	^{28}EKNGIDIYSL
42 kDa	^{645}RGWNRQAGAAGSRM	Not generated
37 kDa	^{689}RLAILPASAP	^{690}LAILPASAP

C

Protease	Type	Biological role	ITIH4 cl.	Cleavage site
Thrombin	Ser	Coagulation	+	R^{644}-R^{645}
Kallikrein	Ser	Coagulation	+	R^{688}-R^{689}
Plasmin	Ser	Fibrinolysis	+	K^{224}-S^{225} + R^{688}-R^{689}/R^{689}-L^{690}
tPa	Ser	Fibrinolysis	–	–
MMP-3	Me^{2+}	Extracellular matrix	(+)	A^{639}-S^{640} + N^{713}-M^{714}
MMP-7	Me^{2+}	Extracellular matrix	+	K^{496}-L^{497} + N^{713}-M^{714}
MMP-13	Me^{2+}	Extracellular matrix	+	N^{713}-M^{714}
C1r	Ser	Complement	–	–
C1s	Ser	Complement	(+)	K^{633}-I^{634} + R^{657}-M^{658}
ADAMTS-4	Me^{2+}	Extracellular matrix	(+)	G^{652}-A^{653} + P^{688}-F^{687}
ADAMTS-5	Me^{2+}	Extracellular matrix	(+)	G^{652}-A^{653}
ADAMTS-13	Me^{2+}	Processing of vWF	–	–
HtrA1	Ser	Protein quality control	–	–
HNE	Ser	Inflammation	(+)	A^{691}-I^{692}
Papain	Cys	-	+	V^{561}-S^{562} + T^{589}-S^{590}

D

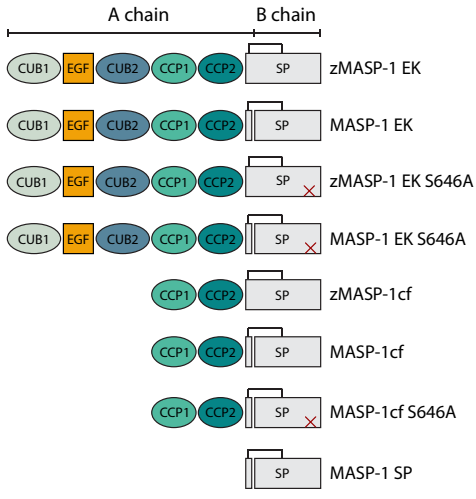

E

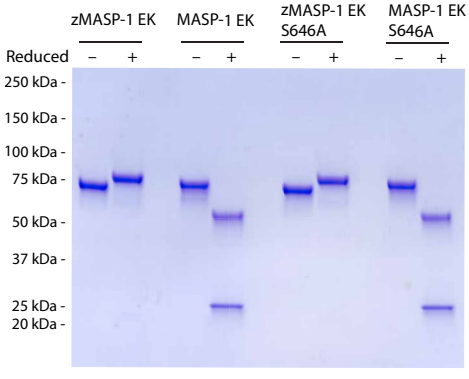

F

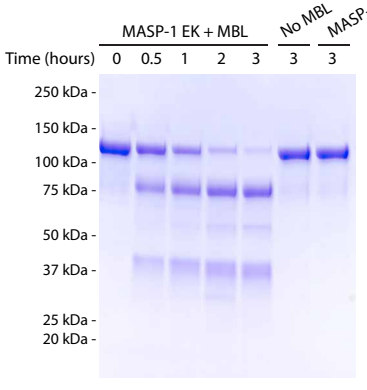

G

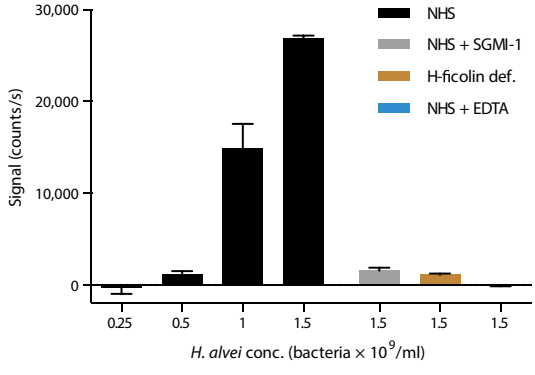

Fig. 2. ITIH4 is a substrate for a diverse set of proteases. (**A**) ITIH4 was incubated with different MASPs and cleavage was followed by SDS-PAGE analysis. Arrows indicate the generated ITIH4 fragments. (**B**) N-terminal sequences of the ITIH4 fragments that are produced by MASP-1cf and MASP-2cf. (**C**) Cleavage of ITIH4 by different proteases. In the ITIH4 cl. column, proteases are divided into those that cleave ITIH4 (+), those that display low levels of cleavage upon longer incubation times (+), and those that do not cleave ITIH4 (–). The cleavage sites are listed by denoting the P1-P1′ residues. (**D**) The domain structures of the MASP-1 variants that are used throughout this study. The disulfide bonds that link the A and B chain are represented by lines, while the S646A mutation is shown by a red cross. (**E**) SDS-PAGE analysis of full-length MASP-1 variants. (**F**) Surface-bound MASP-1 EK cleaves ITIH4. MBL–MASP-1 EK was bound to a mannose solid phase, and ITIH4 cleavage was followed by SDS-PAGE analysis. A sample without MBL and a MASP-1 EK S646A sample served as negative controls. (**G**) *H. alvei* induces formation of ITIH4–MASP-1 complexes in serum. Different *H. alvei* concentrations were added to serum, and ITIH4–MASP-1 complexes were detected using an immunoassay (fig. S4, A and B). Serum from an H-ficolin–deficient patient was used as a control together with the MASP-1 inhibitor SGMI-1 and EDTA ($n = 3$). All data are representative of three repeated experiments. NHS, normal human serum.

(residues 633 to 713) of ITIH4. These results show that a number of different proteases cleave ITIH4, indicating that ITIH4-protease interactions are not restricted to MASP-1 and MASP-2.

ITIH4–MASP-1 complexes are generated during solid-phase LP activation

We decided to use MASP-1 and MASP-2 as model enzymes for studying the interaction between proteases and ITIH4 in detail. Although LP activation is ultimately a surface phenomenon, it becomes a fluid phase event when MASP-1cf and MASP-2cf are used since these truncated variants lack the ability to bind to PRMs. This could have implications for the experimental results, as, e.g., α_2M is known to inhibit MASPs in solution but not on a surface due to the steric restrictions imposed by the solid phase (*20*, *22*). To circumvent this limitation, we generated activated, full-length MASP-1 variants that enable the formation of surface-bound MASP-1–PRM complexes. The domain structure of such variants and the other MASP-1 variants used in the present study are depicted in Fig. 2D. In vitro activation of MASP-1 was facilitated by replacing the natural activation site of MASP-1 and MASP-1 S646A with an enterokinase cleavage site. The zymogenic zMASP-1 EK and zMASP-1 EK S646A variants were purified and, subsequently, activated by enterokinase to produce the cleaved MASP-1 EK and MASP-1 EK S646A variants. Activation of MASP-1 EK was verified by SDS-PAGE since activated MASP-1 migrates as two distinct bands corresponding to the A chain (CUB1-EGF-CUB2-CCP1-CCP2) and B chain (SP domain) under reducing conditions (Fig. 2, D and E). MASP-1 EK was enzymatically active and cleaved ITIH4 with similar kinetics as MASP-1cf (fig. S2E).

To investigate whether ITIH4 is a substrate for MASPs during LP activation, MBL was immobilized on a mannose surface, and cleaved MASP-1 EK or MASP-1 EK S646A were added to form ligand-bound MBL–MASP-1 complexes. When these complexes were incubated with ITIH4, MASP-1 EK time-dependently cleaved ITIH4, whereas no cleavage was observed using the proteolytically inactive MASP-1 EK S646A variant (Fig. 2F). Furthermore, no cleavage was observed in the absence of MBL, emphasizing that ITIH4 cleavage was mediated by PRM-bound MASP-1. Having established that ITIH4 is capable of interacting with MASPs during LP activation, we wanted to examine whether ITIH4–MASP-1 complexes are formed between the endogenous serum proteins on a biologically relevant surface. Because this required a more sensitive technique for detecting ITIH4–MASP-1 complexes, we developed sandwich immunoassays for measuring complex formation. These assays showed that complex formation in serum depended on the concentration of MASP-1cf and the concentration of ITIH4 (fig. S4, A to D). Moreover, serum containing ITIH4–MASP-1cf complexes was fractionated by size exclusion chromatography (SEC), and the assays were used to directly show that ITIH4–MASP-1 complexes with a markedly increased hydrodynamic volume compared to free ITIH4 are formed in serum (fig. S4E). To trigger LP activation in serum by a physiologically relevant activator, we used *Hafnia alvei*, which is a commensal, Gram-negative bacterium that can act as an opportunistic pathogen and induce bacteremia and sepsis and is known to be recognized by the PRM H-ficolin (*23*). Serum was incubated with *H. alvei*, leading to binding and activation of endogenous H-ficolin–MASP complexes that were, subsequently, eluted from the bacterial surface. These eluates were analyzed for the presence of ITIH4–MASP-1 complexes, and *H. alvei* was found to dose-dependently induce formation of ITIH4–MASP-1 complexes (Fig. 2G). The specific MASP-1 inhibitor *Schistocerca gregaria* protease inhibitor-based MASP-1 inhibitor (SGMI-1) efficiently suppressed complex formation. Furthermore, ITIH4–MASP-1 complexes were absent in H-ficolin deficient serum, and complex formation was prevented by EDTA since H-ficolin binds *H. alvei* Ca^{2+} dependently.

Formation of ITIH4-MASP complexes depends on divalent cations

Evolution has repeatedly used VWF domains to mediate protein-protein interactions in multiprotein complexes (*24*). Often, VWF domains contain a metal ion-dependent adhesion site (MIDAS) that is key for directing protein-protein contacts by coordinating divalent cations. Since the 80-kDa fragment of ITIH4 contains a VWF domain, we asked whether the formation of ITIH4–MASP-1 complexes required divalent cations. To test this, serum was dialyzed against tris-buffered saline (TBS) with EDTA to remove divalent cations followed by removal of EDTA by dialysis against TBS. MASP-1 EK was added to the serum together with various divalent cations, and complex formation was measured using the ITIH4–MASP-1 immunoassay (fig. S4, A and B). Removal of divalent cations completely abolished complex formation, an effect that was rescued by Mg^{2+} and Ni^{2+} but none of the other cations (Fig. 3A), suggesting that an ITIH4 MIDAS site occupied with a divalent metal ion, which is likely Mg^{2+} in physiological settings, is required for the interaction. In addition, an increase of the Mg^{2+} concentration in normal human serum led to formation of more ITIH4–MASP-1 complexes.

To ensure that the requirement for Mg^{2+}/Ni^{2+} was not due to an indirect effect in serum, purified ITIH4 was incubated with MASP-1cf in different buffers and fractionated by SEC. When the incubation and SEC were performed in TBS and 2 mM $CaCl_2$ (Ca^{2+}), ITIH4 was cleaved but no stable association of ITIH4 and MASP-1 was observed, as demonstrated by the peaks corresponding to free 80-kDa ITIH4, 37-kDa ITIH4, and free MASP-1cf (Fig. 3B). By contrast, incubation and SEC in TBS, 2 mM $CaCl_2$, and 1 mM $MgCl_2$ (Ca^{2+}/Mg^{2+}) resulted in formation of multiple, early-eluting peaks. SDS-PAGE analysis demonstrated that these peaks were ITIH4–MASP-1 complexes composed of 80/60-kDa ITIH4 and MASP-1cf (fig. S5A). The ratio between ITIH4 and MASP-1cf was stable across the complex-containing peaks, indicating that ITIH4–MASP-1cf constituted a repeating unit that attained different oligomeric states. Currently, it is not known whether ITIH4–MASP-1 oligomerization is physiologically relevant or whether similar oligomers are formed in serum. Mg^{2+} was required at the time of cleavage since no complexes were formed when ITIH4 was cleaved by MASP-1cf in Ca^{2+}, Mg^{2+} was added after cleavage, and SEC was performed in Ca^{2+}/Mg^{2+} (Fig. 3B). Once complexes were formed, neither EDTA nor 1 M NaCl was able to dissociate them (Fig. 3B and fig. S5B), resembling the EDTA- and salt-resistant C3 convertase of the CP and LP (*24*). Moreover, Ni^{2+} was confirmed to support complex formation using purified proteins (fig. S5C). Full-length, dimeric MASP-1 EK and MASP-2cf also produced Mg^{2+}-dependent complexes with ITIH4 of different oligomeric sizes (fig. S5, D and E). The efficiency of complex formation was comparable for MASP-1 and MASP-2, suggesting that the more pronounced complex formation, which was observed for MASP-1 in serum (Fig. 1C), was likely caused by a more effective anti–MASP-1 IP. Although Mg^{2+} was found to be key for forming stable complexes, Mg^{2+} had minimal impact on the cleavage of ITIH4 since MASP-1cf cleaved ITIH4 with similar kinetics in Ca^{2+} and Ca^{2+}/Mg^{2+} (fig. S5F). To assess whether Mg^{2+}-dependent binding to ITIH4 is unique to

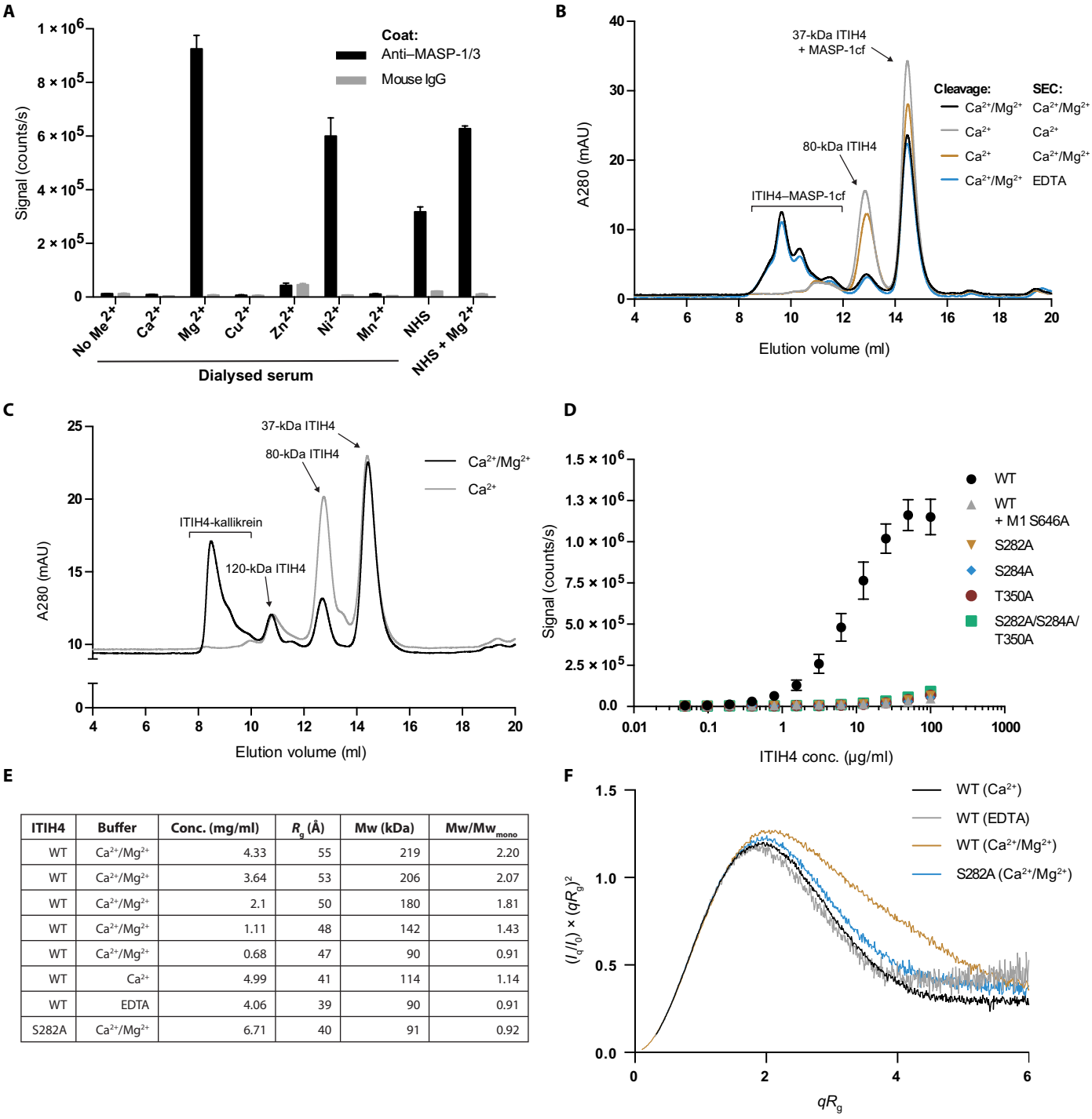

ITIH4	Buffer	Conc. (mg/ml)	R_g (Å)	Mw (kDa)	Mw/Mw$_{mono}$
WT	Ca^{2+}/Mg^{2+}	4.33	55	219	2.20
WT	Ca^{2+}/Mg^{2+}	3.64	53	206	2.07
WT	Ca^{2+}/Mg^{2+}	2.1	50	180	1.81
WT	Ca^{2+}/Mg^{2+}	1.11	48	142	1.43
WT	Ca^{2+}/Mg^{2+}	0.68	47	90	0.91
WT	Ca^{2+}	4.99	41	114	1.14
WT	EDTA	4.06	39	90	0.91
S282A	Ca^{2+}/Mg^{2+}	6.71	40	91	0.92

Fig. 3. The ITIH4 VWF domain is essential for complex formation. (**A**) Complex formation in serum depends on divalent cations. Cations were removed by dialysis, and serum was reconstituted with MASP-1 EK and the indicated cations. ITIH4–MASP-1 was detected using an immunoassay with anti–MASP-1–coated or mouse IgG–coated wells (fig. S4, A and B) ($n = 3$). (**B**) Formation of complexes in a purified system. ITIH4 was cleaved by MASP-1cf, diluted in buffer, and analyzed by SEC. Different buffers were used for the cleavage step and for dilution and chromatography (SEC): TBS and 2 mM $CaCl_2$ (Ca^{2+}); TBS, 2 mM $CaCl_2$, and 1 mM $MgCl_2$ (Ca^{2+}/Mg^{2+}); and TBS and 10 mM EDTA (EDTA). The shown chromatograms are representative of three repeated experiments. (**C**) Kallikrein form Mg^{2+}-dependent complexes with ITIH4. ITIH4 was cleaved by kallikrein in either Ca^{2+} or Ca^{2+}/Mg^{2+} and analyzed by SEC. The chromatogram is representative of three repeated experiments. (**D**) ITIH4 VWF mutants do not form complexes with MASP-1. MASP-1 EK or MASP-1 EK S646A were mixed with ITIH4 variants, and ITIH4–MASP-1 complexes were measured as in (A) ($n = 3$). (**E** and **F**) Small-angle x-ray scattering (SAXS) analysis of ITIH4 or ITIH4 S282A in the buffers described in (B). (E) Estimated parameters from SAXS analysis. Mw/Mw$_{mono}$ is the ratio between the molecular weight of the sample and the average weight of all measurements on monomeric ITIH4. (F) R_g-normalized Kratky plot. mAU, milli-absorbance units.

MASP-1 and MASP-2, we incubated ITIH4 with plasma kallikrein in either Ca^{2+} or Ca^{2+}/Mg^{2+} and analyzed the samples by SEC. As for MASP-1/2, early-eluting complexes of varying oligomeric state were formed in Ca^{2+}/Mg^{2+} (Fig. 3C), and the presence of kallikrein in these fractions was verified by anti-kallikrein WB (fig. S5G). This demonstrates that ITIH4 forms complexes with several distinct proteases and suggests that complex formation may be a general result of cleavage within the PSR.

Mutation of the ITIH4 MIDAS completely prevents complex formation

To directly assign the importance of divalent cations for complex formation to the VWF domain of ITIH4, we identified the cation-chelating residues in ITIH4 using its sequence homology to proteins with available structures of their VWF domains in cation-bound states (fig. S6A). This identified a canonical MIDAS site in ITIH4 containing five residues that are likely key for coordinating the Mg^{2+}/Ni^{2+} ion, and we expressed the charge-neutral mutants ITIH4 S282A, ITIH4 S284A, ITIH4 T350A, and ITIH4 S282A/S284A/T350A. Although these mutants were all efficiently cleaved by MASP-1 EK (fig. S6B), none of them were able to form complexes with MASP-1 EK (Fig. 3D). Furthermore, ITIH4 S282A and ITIH4 S282A/S284A/T350A were purified and incubated with MASP-1cf to examine their complex-forming abilities by SEC, which confirmed the complete loss of complex formation for these mutants (fig. S6C), demonstrating that cation binding by the MIDAS is essential for complex formation.

To probe whether binding of Mg^{2+} by the VWF domain has consequences on the global conformation of ITIH4, small-angle x-ray scattering measurements were made on ITIH4 in TBS buffers supplemented with different divalent cations or EDTA. The molecular weight and the radius of gyration (R_g), which is a measure of protein size, were estimated by Guinier analysis. This showed that the R_g of ITIH4 at 0.68 mg/ml was substantially larger in Ca^{2+}/Mg^{2+} than in Ca^{2+} or EDTA (Fig. 3E). This strongly suggests that binding of Mg^{2+} induces decompaction of ITIH4. By contrast, the dimensions of ITIH4 S282A were not affected by Mg^{2+} availability, highlighting that Mg^{2+}-induced decompaction was mediated directly through the MIDAS. Unexpectedly, ITIH4 was observed to dimerize in Ca^{2+}/Mg^{2+} at supraphysiological concentrations (>0.68 mg/ml). Dimerization was also mediated by the VWF domain, as no dimers were observed even at high concentrations for ITIH4 in Ca^{2+}, ITIH4 in EDTA, or ITIH4 S282A in Ca^{2+}/Mg^{2+} (Fig. 3E). ITIH1 also displays VWF-dependent homodimerization, suggesting that this feature is conserved among ITIHs (*25*). The propensity of ITIH4 to self-associate may be augmented by cleavage and complex formation with proteases, which could explain the various ITIH4-MASP oligomers that were observed by SEC (Fig. 3, B and C). The R_g-normalized Kratky plots of ITIH4 indicate that ITIH4 is a largely globular protein that contains some inherent flexibility without MIDAS-bound Mg^{2+} (Fig. 3F). In contrast, the Kratky plot of monomeric wild-type (WT) ITIH4 in Ca^{2+}/Mg^{2+} displays a slight increase in peak height and a slower monotonic decrease at large q values, which is indicative of an increase in flexibility and disorder, consistent with the larger R_g value.

Complex formation requires a catalytically active SP domain of MASP-1

The various MASP-1 variants (Fig. 2D) were used to delineate the importance of the distinct domains and activation state of MASP-1 for binding ITIH4 by adding them to serum and measuring the extent of complex formation. Using the full-length MASP-1 EK variants, dose-dependent complex formation was seen for the active MASP-1 EK, while neither MASP-1 EK S646A, zMASP-1 EK, nor zMASP-1 EK S646A bound ITIH4 (Fig. 4A). This emphasized that catalytically competent and activated MASP-1 was a prerequisite for generating ITIH4–MASP-1 complexes, which was supported by IP and WB analysis (fig. S7A). MASP-1cf and MASP-1 SP were also found to bind ITIH4, whereas zMASP-1cf and MASP-1cf S646A did not (Fig. 4B). To confirm these results, MASP-1cf and MASP-1 SP were added to serum, immunoprecipitated with anti-ITIH4, and analyzed by anti–MASP-1 WB. Again, both MASP-1 fragments were found to support complex formation (Fig. 4C). The fact that the SP domain of MASP-1 was sufficient for forming complexes with ITIH4 indicates that the CCP domains do not contain any key exosites, which is supported by the similar ITIH4 cleaving rates of MASP-1cf and MASP-1 SP (fig. S7B).

To obtain low-resolution structures of ITIH4 and the ITIH4–MASP-1 complex, we performed negative stain electron microscopy (nsEM). Initially, we analyzed intact ITIH4 by itself, yielding a three-dimensional (3D) reconstruction in which the recently deposited crystal structure of ITIH1 (Protein Data Bank entry 6FPY) fitted reasonably (fig. S7, C and D). The crystallized fragment of ITIH1 corresponds roughly to the 80-kDa ITIH4 segment, and these ITIH1 and ITIH4 fragments display 38% sequence identity. To analyze ITIH4–MASP-1cf, we generated complexes as in Fig. 3B, and the peak fraction of monomeric ITIH4–MASP-1 eluting at 11.6 ml, was chosen for nsEM. Analysis of nsEM data yielded 2D classes in which the individual domains of the MASP-1 fragment were clearly visible (fig. S7E) and the crystal structure of MASP-1cf could be fitted with confidence into the nsEM 3D reconstruction. Although the crystal structure of ITIH1 fits within the nsEM density of intact ITIH4, it could not be matched in a satisfying manner with the density that was not assigned to MASP-1cf in the ITIH4–MASP-1 complex (Fig. 4D and fig. S7F). In the complex, the ITIH4 density seems to open up to create a hole that is occupied by two helices of ITIH1. This suggests that the 80-kDa ITIH4 fragment undergoes a structural rearrangement to support formation of ITIH4–MASP-1 complexes with a relatively small interface that is restricted to the SP domain of MASP-1.

ITIH4 inhibits proteases without perturbing their active sites

We hypothesized that the formation of ITIH4-protease complexes inhibits the proteolytic activity of the enzyme. Initially, we purified ITIH4–MASP-1cf complexes and compared their catalytic activity to free MASP-1cf using the small peptide substrate methylsulfonyl-D-Phe-Gly-Arg conjugated to 7-amino-4-methyl coumarin (FGR-AMC). MASP-1 activity was quantified as the increase in AMC fluorescence, and the initial rates were determined by linear regressions (fig. S8, A and B). Unexpectedly, there was no difference in activity between free MASP-1cf and ITIH4–MASP-1cf (Fig. 5A). Although these results highlight that the active site of MASP-1 remains intact within ITIH4-MASP-1 complexes it still leaves the possibility that ITIH4 exerts an inhibitory effect by physically restricting access to the active site for larger protein substrates. Since MASP-1 cleaves C2 during LP activation, free MASP-1cf and ITIH4–MASP-1cf were incubated with purified C2, and cleavage was monitored by SDS-PAGE (fig. S8C). C2 cleavage was quantified by densitometry, and ITIH4–MASP-1cf was found to cleave C2 threefold slower than free MASP-1cf ($t_{1/2}$ values were 23.7 and 73.3 min for MASP-1cf and ITIH4–MASP-1cf, respectively) (Fig. 5B).

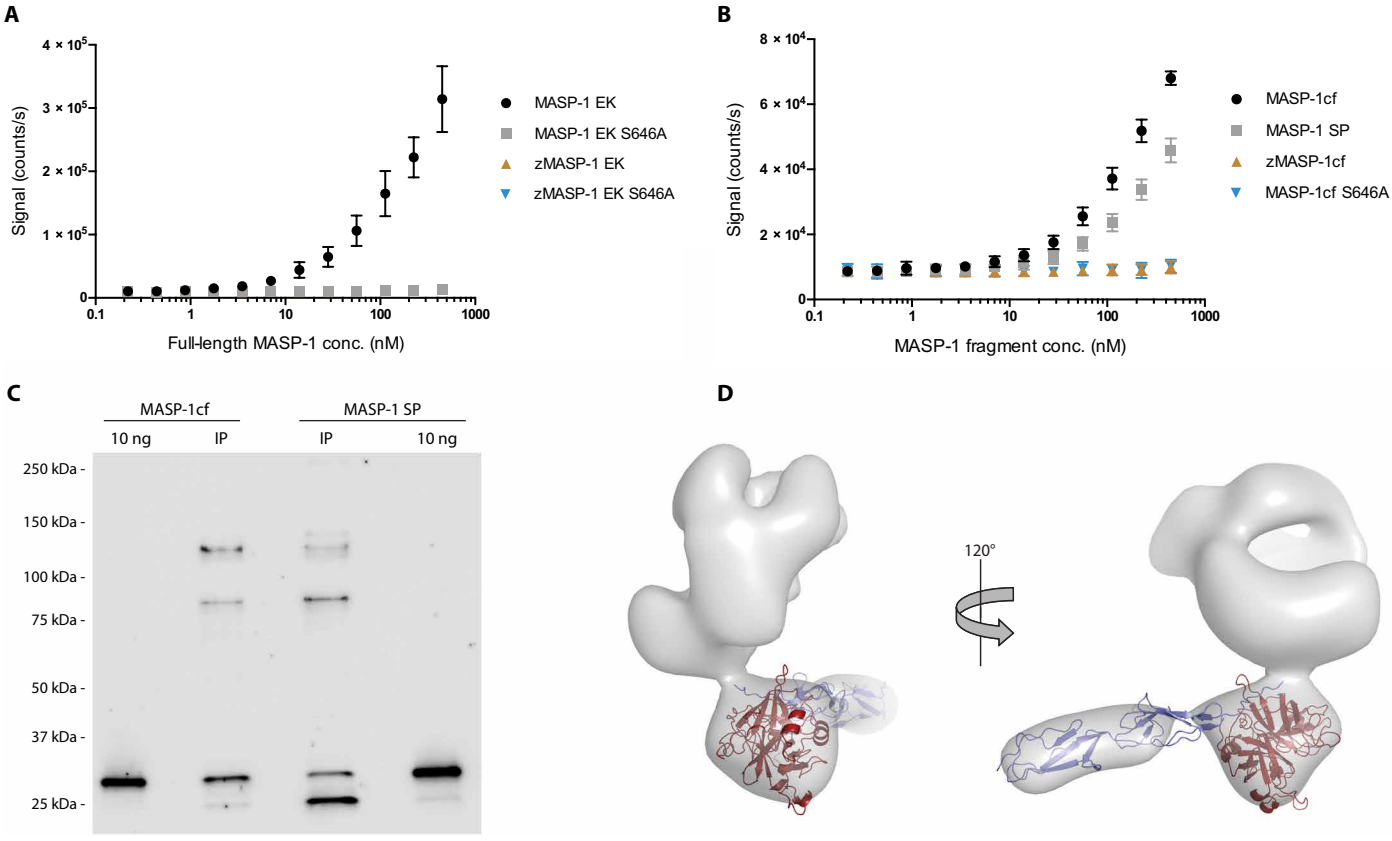

Fig. 4. An active MASP-1 SP domain is sufficient for complex formation. (**A** and **B**) An active MASP-1 SP domain is sufficient for complex formation. (A and B) Complex formation with full-length MASP-1 (A) or MASP-1 fragments (B). MASP-1 variants were added to NHS, and ITIH4–MASP-1 complexes were detected using the immunoassay (fig. S4, A and B). Note that the data points for MASP-1 EK S646A, zMASP-1 EK, and zMASP-1 EK S646A in (A) are all at a background level ($n = 3$). (**C**) WB analysis of complex formation using MASP-1cf and MASP-1 SP. MASP-1 was added to serum, immunoprecipitated with anti-ITIH4, and analyzed by anti–MASP-1 WB. The bands at 120 and 85 kDa are covalent complexes between MASP-1 and α_2M and/or C1inh and α_2M and/or antithrombin, respectively. The bands at 22 kDa are due to autodegradation of MASP-1, which was more pronounced for MASP-1 SP than for MASP-1cf. The WB is representative of three repeated experiments. (**D**) 3D reconstitution of nsEM particles of ITIH4–MASP-1cf complexes. The deposited crystal structure of MASP-1cf (Protein Data Bank: 3GOV) is fitted into the envelope with the SP domain shown in red and the CCP1 and CCP2 domains depicted in purple.

Next, the effect of ITIH4 on MASP-2 activity was assessed by exploiting that Mg^{2+} is required for the formation of ITIH4–MASP-2 complexes, whereas ITIH4 cleavage is Mg^{2+} independent. MASP-2cf was incubated with ITIH4 in either Ca^{2+}/Mg^{2+} or Ca^{2+} or incubated in Ca^{2+}/Mg^{2+} in the absence of ITIH4. After complete ITIH4 cleavage, the samples were incubated with FGR-AMC and, as for MASP-1, the activity of MASP-2 against the small peptide substrate was not affected by the formation of ITIH–MASP-2 complexes (Fig. 5C and fig. S8D). To examine the activity of ITIH4–MASP-2 complexes against protein substrates, we initially focused on cleavage of C4. During LP activation, MASP-2 is the only protease that cleaves C4, generating C4b that contains a thioester that covalently links it to the target surface. As in Fig. 5C, ITIH4 was cleaved by MASP-2cf, and MASP-2 was, subsequently, captured in microtiter wells using an anti–MASP-2 antibody. Then, purified C4 was added to the wells, and MASP-2 activity was estimated as the deposition of C4 fragments in the well. This showed that 18-fold higher concentrations of ITIH4–MASP-2cf was required for obtaining half of the maximum C4 deposition than for free MASP-2cf (72.6 pM versus 3.97 pM for MASP-2cf) (Fig. 5D), highlighting that ITIH4 inhibits both MASP-1 and MASP-2 by obstructing access to their active sites. Since C4b deposition is an indirect measure of MASP-2 activity, we also directly monitored the effect of ITIH4 on C2 and C4 cleavage by MASP-2 in solution. ITIH4 dose-dependently inhibited MASP-2 with comparable median inhibitory concentration (IC_{50}) values for the two substrates [IC_{50}(C2) = 4.5 μM versus IC_{50}(C4) = 5.6 μM] (Fig. 5E). Noticeably, the molar excess of ITIH4 at these concentrations is approximately 22-fold, which is considerably lower than the molar ratio between ITIH4 and MASP-2 in serum (360-fold excess of ITIH4 assuming ITIH4 at 200 μg/ml) (*12*). The ITIH4-mediated inhibition of MASP-2 was also evident over time at a fixed ITIH4 concentration, resulting in approximately eightfold slower cleavage of C2 and C4 in Ca^{2+}/Mg^{2+} compared to Ca^{2+} (fig. S7, E and F). Thus, ITIH4 inhibited MASP-2cf more efficiently than MASP-1cf in this setup. In summary, ITIH4 inhibited the activity of both MASP-1 and MASP-2 against two distinct, highly-relevant protein substrates but not against smaller peptide substrates. Since plasma kallikrein also formed complexes with ITIH4 (Fig. 3C), we examined whether kallikrein-mediated cleavage of the substrate HMWK is inhibited by ITIH4. As for MASP-1/2, dose-dependent inhibition was observed in Ca^{2+}/Mg^{2+}, whereas ITIH4 had no effect on kallikrein activity in the absence of Mg^{2+}. The IC_{50} of ITIH4-mediated inhibition was 0.09 μM, corresponding to a 4.7-fold molar excess of ITIH4 over kallikrein, which is comparable to the 3.4-fold molar excess of ITIH4 compared to prekallikrein in plasma (*26*).

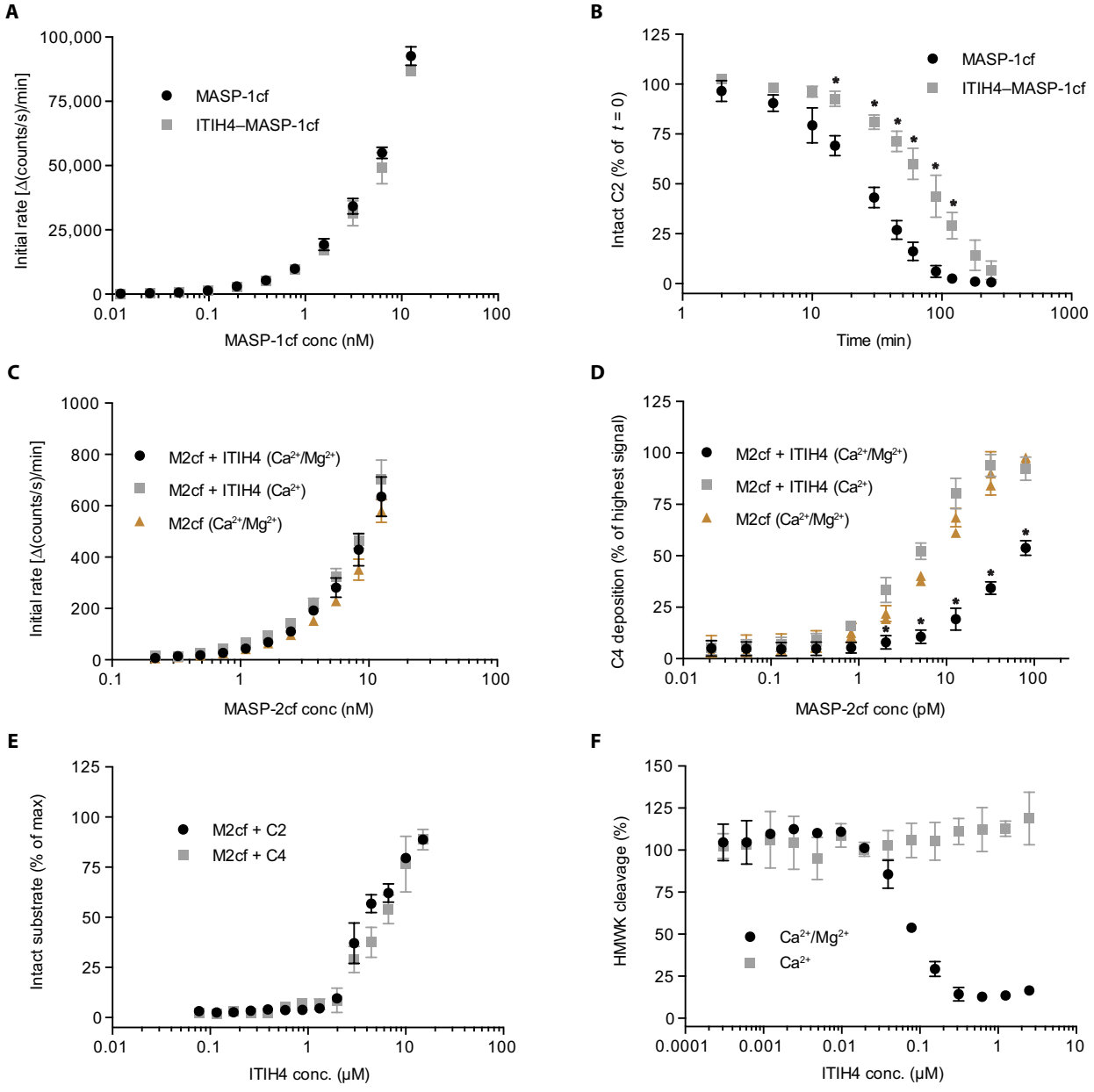

Fig. 5. ITIH4 inhibits proteases without disrupting their active sites. (**A** and **B**) ITIH4–MASP-1cf complexes were purified by SEC, and their activity was compared to that of free MASP-1cf. (A) Cleavage of FGR-AMC by MASP-1 at various concentrations of MASP-1cf and ITIH4–MASP-1cf. The initial rates were estimated and plotted against the concentration of MASP-1cf (fig. S8, A and B) ($n = 3$). (B) C2 cleavage by MASP-1cf and ITIH4–MASP-1cf. The cleavage of C2 was monitored by SDS-PAGE (fig. S8C) and quantified using densitometry ($n = 3$). (**C** and **D**) To form ITIH4–MASP-2cf complexes, MASP-2cf was incubated with or without ITIH4 in TBS and 2 mM $CaCl_2$ (Ca^{2+}) or TBS, 2 mM $CaCl_2$, and 1 mM $MgCl_2$ (Ca^{2+}/Mg^{2+}). (C) Cleavage of FGR-AMC by MASP-2. Linear rates were estimated as in (A) (fig. S8D) ($n = 3$). (D) Cleavage of C4 by MASP-2. After incubation with ITIH4, the samples were added to anti–MASP-2–coated wells. C4 was added to the wells, and C4 deposition was quantified using anti-C4. In (A to D), the mean values at each MASP concentration were compared using multiple t tests with Holm-Sidak adjustment for multiple comparisons ($\alpha = 0.05$). In (C and D), M2cf + ITIH4 (Ca^{2+}/Mg^{2+}) and M2cf + ITIH4 (Ca^{2+}) were compared statistically. Asterisks denote statistically significant differences ($n = 3$). (**E**) ITIH4 dose-dependently inhibits MASP-2cf–mediated cleavage of C2 and C4. Substrate cleavage was analyzed by SDS-PAGE and quantified by densitometry (fig. S8, G and H) ($n = 2$). (**F**) ITIH4 inhibits cleavage of HMWK by plasma kallikrein. Cleavage was monitored by SDS-PAGE by following the generation of the H and L chain (fig. S8, I and J) ($n = 2$).

These results demonstrate that ITIH4 efficiently inhibits the activity of proteases upon complex formation.

ITIH4-MASP complexes inhibit LP activation in serum

Having established that ITIH4 can inhibit MASP-1 and MASP-2 in purified systems, we investigated the effect of ITIH4 on LP activity mediated by endogenous PRM-MASP in serum. Microtiter wells can be coated with different ligands that selectively drive complement activation through distinct PRMs. Serum was mixed with varying concentrations of ITIH4 and added to mannan-coated wells to induce MBL-driven LP activation. LP activity was quantified as the covalent deposition of C4 and C3 fragments onto the surface, reflecting

MASP-2–mediated C4 cleavage and C3 cleavage by the LP C3 convertases, respectively. ITIH4 efficiently and dose-dependently inhibited C4 and C3 deposition, whereas human serum albumin (HSA) had no effect on LP activity (Fig. 6, A and B). ITIH4 was a less potent inhibitor of the LP than the well-characterized, major physiological inhibitor C1inh (Fig. 6, A to C). Since ITIH4 S282A and ITIH4 S282A/S284A/T350A were cleaved by MASPs but were not able to form ITIH4-MASP complexes, they enabled us to discriminate between LP inhibition by a competitive substrate effect and inhibition due to complex formation. The ITIH4 mutants had no effect on LP activity, highlighting that LP inhibition required formation of ITIH4-MASP complexes. This was further verified by isolating MBL-MASP complexes from serum on a mannan surface and incubating them with purified C4 and ITIH4, showing that ITIH4 only inhibited C4 deposition in a Mg^{2+}-containing buffer, while C1inh inhibited LP activity regardless of the buffer composition (fig. S9A). Furthermore, ITIH4 exerted minimal impact on the binding of MASPs to MBL and on the binding of MBL to mannan (fig. S9B).

Because the LP can be initiated by several PRMs, the effect of ITIH4 was also assessed in an assay that uses acetylated bovine serum albumin (BSA) to initiate H-ficolin–driven LP activation. Again, ITIH4 robustly inhibited C3 and C4 deposition, and the inhibitory efficiency was only slightly lower than that of C1inh on this surface (Fig. 6C and fig. S9, C and D). In contrast to the LP, no effect of

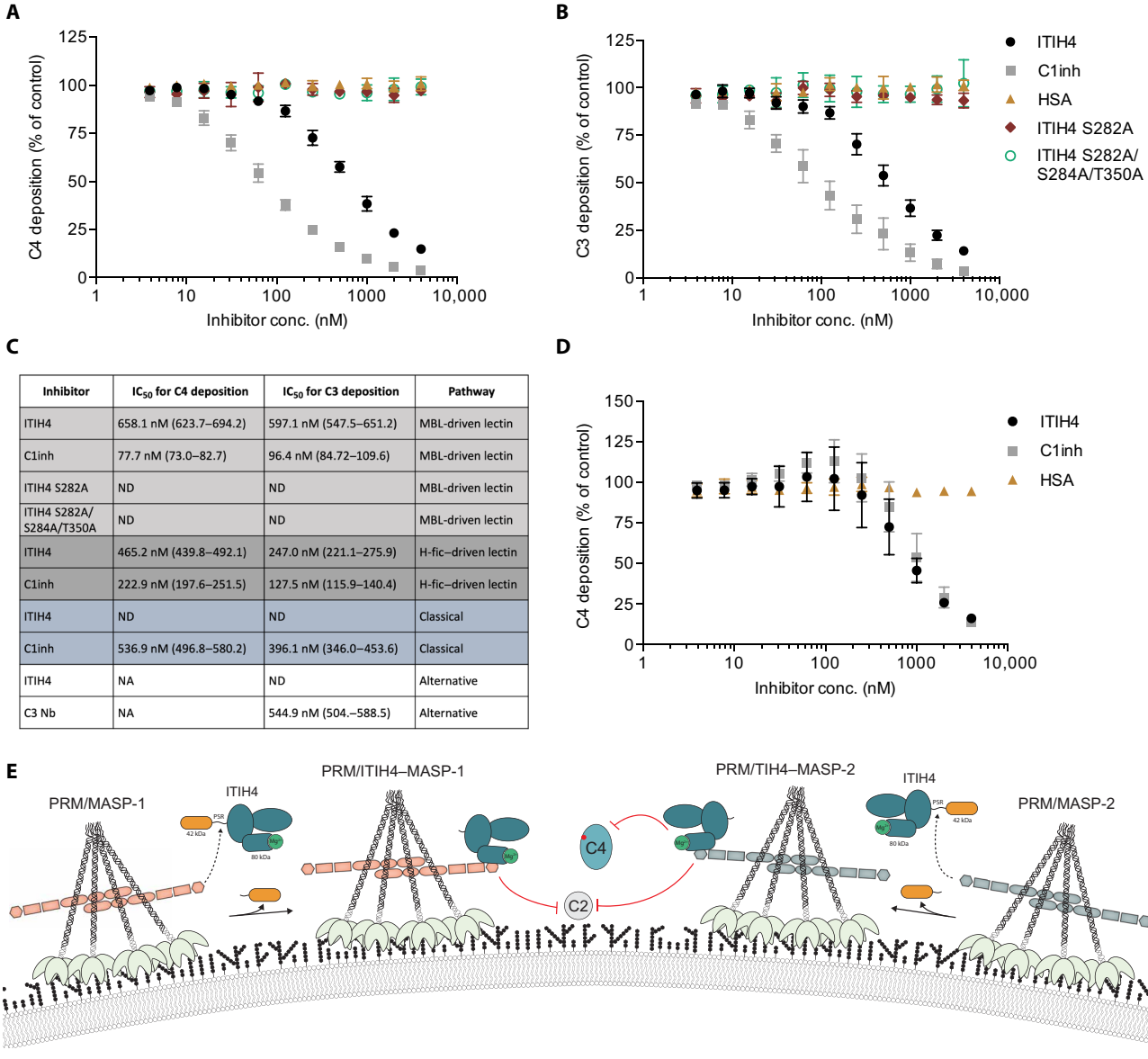

Inhibitor	IC_{50} for C4 deposition	IC_{50} for C3 deposition	Pathway
ITIH4	658.1 nM (623.7–694.2)	597.1 nM (547.5–651.2)	MBL-driven lectin
C1inh	77.7 nM (73.0–82.7)	96.4 nM (84.72–109.6)	MBL-driven lectin
ITIH4 S282A	ND	ND	MBL-driven lectin
ITIH4 S282A/ S284A/T350A	ND	ND	MBL-driven lectin
ITIH4	465.2 nM (439.8–492.1)	247.0 nM (221.1–275.9)	H-fic–driven lectin
C1inh	222.9 nM (197.6–251.5)	127.5 nM (115.9–140.4)	H-fic–driven lectin
ITIH4	ND	ND	Classical
C1inh	536.9 nM (496.8–580.2)	396.1 nM (346.0–453.6)	Classical
ITIH4	NA	ND	Alternative
C3 Nb	NA	544.9 nM (504.–588.5)	Alternative

Fig. 6. ITIH4 inhibits the LP in human and murine serum. (**A** and **B**) Varying concentrations of the indicated proteins were added to serum, and the LP was activated in mannan-coated wells. LP activity was quantified at the level of C4 (A) and C3 (B) ($n = 3$). (**C**) IC_{50} values for inhibition of the LP, CP, or AP. IC_{50} values were derived from (A) and (B) or fig. S9 by nonlinear regressions that fitted with $R^2 > 0.75$. ND signifies that the regression did not converge, whereas NA indicates that the data are not available. (**D**) ITIH4 inhibits the LP in murine serum. As in (A) but using serum from C57BL/6 mice ($n = 3$). (**E**) Inhibitory mechanism of ITIH4. MASP-1 and MASP-2 are activated upon binding of PRMs to target surfaces. Activated MASP-1 and MASP-2 cleave ITIH4 within the PSR, leading to complex formation between the MASP and the 80-kDa ITIH4 fragment. By contrast, the 42/37-kDa ITIH4 fragment dissociates into the fluid phase. Complex formation inhibits cleavage of the downstream proteins C2 and C4, thereby inhibiting the LP.

ITIH4 was observed on CP and AP activity (Fig. 6C and fig. S9, E to G). Thus, ITIH4 specifically targets the LP within the complement system. Human ITIH4 also inhibited MBL-driven LP activity in murine serum, and the efficiency was equal to that of human C1inh (Fig. 6D). Conversely, human MASP-1cf formed complexes with endogenous murine ITIH4 (fig. S9H), suggesting that ITIH4 inhibits the LP by a novel inhibitory mechanism that is evolutionarily conserved (Fig. 6E).

DISCUSSION

ITIH4 is an abundant plasma protein that is cleaved in a number of different pathologies but has evaded extensive scrutiny, partly because its biological role has been unknown. Here, we show that ITIH4 is cleaved within a PSR by various proteases. For the plasma proteases MASP-1, MASP-2, and plasma kallikrein, which promote inflammation by activating the complement and kallikrein-kinin systems, respectively, cleavage of ITIH4 results in the formation of noncovalent ITIH4-MASP complexes and protease inhibition by a previously undescribed mechanism.

Formation of ITIH4-MASP complexes translated into inhibition of LP-driven complement activation (Fig. 6and fig. S9). Despite the residual activity that we observe for ITIH4-MASP complexes (Fig. 5 and fig. S8), ITIH4 almost completely inhibited C4 and C3 deposition in the LP activity assays (Fig. 6 and fig. S9). This may be explained by a synergistic effect of ITIH4 since it targets five different reactions during LP activation: (i) activation of MASP-1 by MASP-1, (ii) activation of MASP-2 by MASP-1, (iii) cleavage of C2 by MASP-1, (iv) cleavage of C2 by MASP-2, and (v) cleavage of C4 by MASP-2. ITIH4 selectively inhibited the LP within the complement system, as no effect was seen on the CP or the AP (Fig. 6). By contrast, it was previously suggested that ITIH1 and/or ITIH2, which form covalent proteoglycan complexes with bikunin, can inhibit all three complement pathways through a combination of several distinct but ill-defined mechanisms (*27*). Similarly, ITIH1 has recently been shown to inhibit the AP by binding to C3 using its VWF domain (*25*). This nonspecific nature of ITIH1/2-mediated complement inhibition is thus markedly different from the LP-specific effect of ITIH4. We note that ITIH4-mediated LP inhibition was less efficient than inhibition by C1inh in our assays, indicating that ITIH4 might not be the main inhibitor of the MASPs under normal physiological conditions. However, the importance of LP inhibitors is context dependent and not fully reflected by their ex vivo potency (*28*). A limitation of our study is that LP inhibition by ITIH4 is not examined in an in vivo model. However, we do provide further lines of evidence supporting the link between ITIH4 and the LP, as we show that ITIH4–MASP-1 complexes are formed in serum by the endogenous proteins upon incubation with *H. alvei* (Fig. 2G). Noticeably, a 35-kDa ITIH4 fragment was observed in patients infected with *M. tuberculosis*, which is known to activate the LP (*29*), that had up-regulated levels of MBL and MASP-2 (*10*). Thus, it is tempting to speculate that infection leads to up-regulation of MBL and MASP-2, which is subsequently activated on the bacterial surfaces, leading to cleavage of ITIH4 and release of the 35-kDa fragment. In addition, we showed formation of ITIH4–MASP-1 complexes and ITIH4-mediated inhibition of the LP in murine serum (Fig. 6D and fig. S9H), demonstrating that the role of ITIH4 as a LP regulator is evolutionarily conserved.

The VWF domain of ITIH4 was key for protease inhibition, as a Mg^{2+}- or Ni^{2+}-bound MIDAS site was required for complex formation (Fig. 3). This indicates that the MIDAS ion, which significantly altered the dimensions of intact ITIH4 (Fig. 3, E and F), induces a conformation that enables postcleavage complex formation. Although VWF domains are exploited by various proteins for mediating protein-protein interactions, this is, to our knowledge, the first example of a VWF domain being directly involved in protease inhibition. All ITIHs contain VWF domains with canonical MIDAS sites, and ITIH1 and/or ITIH2 also rely on their VWF domains for binding to pentraxin 3 (*30*). Thus, the VWF domains are emerging as key domains for protein binding by ITIHs, although the consequences of these binding events are vastly different. In contrast to complex formation, the MIDAS ion did not serve a key role for ITIH4 cleavage (Fig. 3and fig. S5F), highlighting that cleavage and complex formation are two separate events. Unexpectedly, Mg^{2+} was required at the time of cleavage to form ITIH4–MASP-1 complexes, whereas no association was seen when adding Mg^{2+} after cleavage (Fig. 3B). This suggests that the 80-kDa ITIH4 fragment attains a transient conformation capable of protease binding that relaxes into a nonbinding state if a complex is not formed, thereby ensuring that protease inhibition is retained locally in vivo.

ITIH4 was cleaved in vitro by several serine, cysteine, and metalloproteases belonging to different biological systems (Fig. 2C and fig. S3). In addition, a number of proteases were found not to cleave ITIH4, underlining that cleavage of ITIH4 is not a universal protease substrate. The group of noncleaving proteases included ADAMTS-13 and MASP-3, which are extremely specific proteases that circulate as constitutively active enzymes (*15*, *31*). Thus, the lack of ITIH4 cleavage by these proteases is consistent with the fact that ITIH4 was found as a full-length protein in serum (fig. S2, A to C). By mapping the cleavage sites of different human proteases with distinct substrate specificities, we identified a region in ITIH4 that was particularly susceptible to proteolysis (residues 633 to 713), which has previously been termed the PRR (*4*). We suggest that the PRR is redefined as the PSR, as this name holds functional significance. Note that the PSR defined in the present study may be extended in the future, as the cleavage sites of additional proteases are mapped. The susceptibility of the PSR to cleavage may be partly explained by its many prolines (17.3%) because prolines often lead to an overrepresentation of unstructured conformations due to the restrictions that the residue imposes on the main chain conformation (*32*). A limitation of our study is that although the ITIH4-cleaving proteases were all active, we did not perform active site titrations to estimate the exact concentration of functional enzyme. Thus, the ITIH4 cleavage results should mainly be used qualitatively rather than for a detailed enzymological comparison. Still, MASP-1, MASP-2, MMP-7, and MMP-13 appeared to cleave ITIH4 most efficiently (fig. S3). The cleavage by MMP-7 and MMP-13 is intriguing since these proteases are known to be overactive in various types of cancer (*33*), consistent with the fragmentation of the PSR in such patients (*7*). We speculate that the mechanism by which ITIH4 inhibits MASP-1, MASP-2, and kallikrein (Fig. 6E) is generally applicable to proteases that cleave within the PSR. In support of this, we note that these proteases all formed complexes with ITIH4, although their initial cuts were located at different sites in the PSR (Figs. 2C and 2B). However, it remains to be experimentally verified at the level of each individual protease whether cleavage of ITIH4 leads to complex formation and protease inhibition. We anticipate that knowledge about the cleavage site preferences of various proteases will aid in decoding, which protease(s) are responsible for ITIH4 cleavage in different pathologic conditions.

We find that ITIH4-mediated inhibition of MASP-1 and MASP-2 is exerted by a novel inhibitory mechanism. Protease inhibitor mechanisms are generally divided into the standard (canonical), the nonstandard (noncanonical), the serpin, or the α_2M mechanism (*34*). ITIH4 resembles the standard and nonstandard inhibitors by forming noncovalent inhibitor-protease complexes that dissociated during nonreduced SDS-PAGE analysis. By contrast, ITIH4 is mechanistically similar to the serpins and α_2M by requiring cleavage to induce inhibition (Fig. 4). C1inh and α_2M form covalent inhibitor-protease complexes upon cleavage of their reactive center loop or bait region, respectively (*19*, *21*), inferring that the PSR functions similar to these regions. However, the reactive center loop and bait region differ in some important aspects. The α_2M bait region displays great sequence variation across species and can be cleaved in a multitude of different positions to yield inhibitor-protease complexes (*21*). By contrast, the shorter reactive center loop of C1inh is extremely evolutionarily conserved, and cleavage outside of the P1-P1′ position can induce a conformational change in C1inh that does not produce a C1inh-protease complex (*35*). Noticeably, the PSR of ITIH4 displays a high degree of sequence variation among species (*4*), is a rather long segment, and can likely be cleaved in multiple sites to yield inhibitor-protease complexes, as seen for MASP-1, MASP-2, and kallikrein (Figs. 1 to 3). Consequently, the PSR seems to resemble the bait region of α_2M more closely than the C1inh reactive center loop. Furthermore, the serpins and α_2M are known to undergo extensive conformational changes during inhibitor-protease complex formation, whereas minimal changes are seen for standard and nonstandard inhibitors (*34*). Our nsEM analysis of ITIH4 and ITIH4–MASP-1 complexes suggests that the conformation of the 80-kDa fragment of ITIH4 changes upon complex formation (fig. S7). However, we acknowledge that although the nsEM data provide valuable insight into the global architecture of the ITIH4–MASP-1cf complex, higher-resolution structures of the complex will be required to understand in detail how complex formation gives rise to the observed mechanism of protease inhibition. In contrast to serpins and α_2M, cleavage of ITIH4 not only led to protease binding but also released a C-terminal fragment (Fig. 3 and fig. S5). The release of a sizeable protein fragment as a result of inhibitor-protease complex formation constitutes yet another distinctive feature of ITIH4-mediated protease inhibition. In the future, it would be interesting to assess whether the C-terminal ITIH4 fragment serves downstream functions or if it is a passive byproduct that is merely cleared from the circulation.

MASP-1 and MASP-2 inhibition by ITIH4 was mediated by producing complexes that leave the active site of the protease intact but less accessible to larger substrates (Fig. 5). This mimics the α_2M mechanism, as α_2M-trapped proteases are also able to cleave small substrates, while larger protein substrates are physically excluded from the active site (*21*). In contrast to α_2M, which completely enwraps proteases in a molecular cage (*36*), ITIH4 sterically blocks larger substrates from being cleaved by shielding a smaller surface of the MASPs (Fig. 4D). This enables ITIH4 to function as a smaller, monomeric inhibitor, and it can, therefore, inhibit solid-phase LP activation (Fig. 6), which the larger α_2M is not capable of (*20*, *22*). An additional unique feature of ITIH4-mediated inhibition is the fact that residual C2-cleaving activity was still observed for purified ITIH4–MASP-1 complexes (Fig. 5B). This could be explained by dissociation of the complexes after purification, although we find that ITIH4–MASP-1 complexes were extremely stable once formed. An alternative explanation might be that flexibility within the complexes leads to inefficient gatekeeping of access to the active site. Note that the experiments with MASP-2cf did not use purified complexes, meaning that it was not possible to differentiate between residual activity of complexes and incomplete complex formation in these experiments (Fig. 5, C and D). The model in which ITIH4 serves as a gatekeeper for access to the active sites within ITIH4-protease complexes could also explain why ITIH4 inhibited MASP-2cf more efficiently than MASP-1cf (Fig. 5B and fig. S8, E and F), as the active site of MASP-1 is wider and more accessible than that of MASP-2 (*37*).

In summary, we have shown that the plasma protein ITIH4 is a protease inhibitor that may target several proteases by a novel inhibitory mechanism, as exemplified by its inhibition of MASP-1, MASP-2, and kallikrein (Fig. 6E). Following cleavage of the PSR of ITIH4, Mg^{2+}-dependent complexes are formed between the 80-kDa ITIH4 fragment and the executing protease that relies on the ITIH4 VWF domain. The active sites of MASP within the noncovalent ITIH4-MASP complexes are catalytically competent, but downstream cleavage of C2 and C4 are inhibited by physically blocking access of the scissile bonds to the active sites. Such activity was demonstrated in human and murine serum. ITIH4 was found to be cleaved by various proteases within the PSR, suggesting that ITIH4 is a broad-acting inhibitor that targets numerous proteases.

MATERIALS AND METHODS

Co-IP using activated MASPs

Descriptions of recombinant proteins, including activated MASPs, are listed in Supplementary Materials and Methods. IP for mass spectrometry analysis was performed by diluting serum to 12.5% in TBS, 0.05% (v/v) Tween 20, and 5 mM $CaCl_2$ (TBST/Ca^{2+}) together with MASP-1cf, which was added to a final concentration of 82 nM. All steps were performed at 4°C. Following overnight incubation, biotinylated antibody was added (24 μg/ml), and the samples were incubated for 1 hour. Subsequently, streptavidin agarose resin (Thermo Fisher Scientific) was added (10% v/v), and the samples were incubated for 1.5 hours. The beads were washed thrice in TBST/Ca^{2+} and transferred to Pierce Micro-Spin Columns (Thermo Fisher Scientific). Buffer was removed by centrifugation, and elution was performed using 0.1 M glycine (pH 2.5). The pH of the eluates was neutralized using 1 M tris (pH 8.5) (0.06 times the elution volume). In experiments for WB analysis, MASP variants were added to a final concentration of 260 nM, and biotinylated antibodies were used at a concentration of 37 μg/ml. The LC-MS/MS analysis is described in Supplementary Materials and Methods.

IP from serum obtained from WT C57BL/6 mice was performed as IPs from normal human serum (NHS). For pulldown of MASP-1cf variants, MASP-1 EK variants, and MASP-3 K448Q, we used a murine anti–MASP-1/3 antibody. IP of MASP-2cf was performed using a rat anti–MASP-2 antibody, whereas pulldown of ITIH4 was conducted using affinity-purified, polyclonal rabbit anti-ITIH4 antibody (Supplementary Materials and Methods). As isotype controls, biotinylated mouse immunoglobulin G (IgG) (7404304, Lampire), biotinylated rat IgG (7407005, Lampire), or biotinylated rabbit IgG (7406404, Lampire) was used.

WB analysis

Samples were subjected to SDS-PAGE using 4 to 15% Criterion TGX Precast Midi Protein Gels and transferred to nitrocellulose membranes

using the semidry Trans-Blot Turbo Transfer System (Bio-Rad). The membranes were blocked by incubation in TBS and 0.1% (v/v) Tween 20 for 1 hour before addition of the primary antibodies, which were diluted in 25 mM tris, 0.05% (v/v) Tween 20, 1 mM EDTA, HSA (1 mg/ml; CSL Behring), and human IgG (100 μg/ml; Beriglobin, CSL Behring) (pH 7.4). Detection of human ITIH4 was achieved using monoclonal rabbit anti-ITIH4 (0.05 μg/ml; ab180139, Abcam) mixed with polyclonal rabbit anti-ITIH4 (0.05 μg/ml; HPA001835, Sigma-Aldrich), which ensures that both N- and C-terminal fragments of ITIH4 are detected. Murine ITIH4 was detected using monoclonal rabbit anti-ITIH4 (0.1 μg/ml; ab180139, Abcam). MASP-1 was detected using mouse anti–MASP-1 antibody (1 μg/ml); MASP-3 was detected using a monoclonal rat anti–MASP-3 antibody (1 μg/ml), while MASP-2 was detected using polyclonal antiserum (1:1000 dilution) from a rat that was immunized with a MASP-2 fragment. In all cases, the secondary antibody was the appropriate species-specific anti-IgG antibody conjugated with horseradish peroxidase (Dako).

Cleavage of ITIH4 by different proteases

To examine whether ITIH4 was cleaved by the different MASPs, 2000 nM ITIH4 (201 μg/ml) was incubated at 37°C with 100 nM MASP in TBS and 2 mM $CaCl_2$. Aliquots were withdrawn at different time points, and the reaction was stopped by diluting the sample in SDS-PAGE loading buffer. MASP-1cf–mediated cleavage of ITIH4 was performed in both TBS and 2 mM $CaCl_2$ and TBS, 2 mM $CaCl_2$, and 1 mM $MgCl_2$ to examine the effect of Mg^{2+} on the cleavage rate. The samples were separated by SDS-PAGE using 4 to 15% Criterion TGX Precast Midi Protein Gels (Bio-Rad) and stained with Coomassie Brilliant blue R 250 (Merck).

To investigate the cleavage of ITIH4 by different proteases, 2000 nM ITIH4 was incubated with 80 nM protease at 37°C and the reaction was stopped at different time points by mixing aliquots with SDS-PAGE loading buffer containing dithiothreitol (25 mM). Cleavage by serine proteases was performed in TBS, 2 mM $CaCl_2$, and 2 mM $MgCl_2$, whereas cleavage by metalloproteases was performed in 50 mM tris, 150 mM NaCl, 10 mM $CaCl_2$, 2 mM $MgCl_2$, and 0.05% Brij 35 (pH 7.6). The samples were used for Coomassie-stained SDS-PAGE and N-terminal sequencing to identify the cleavage sites of the initial cut. If it was not possible to distinguish the order of two cleavage events for an individual protease, then we mapped both cleavage sites. The N-terminal sequencing and the various proteases are described in Supplementary Materials and Methods.

Cleavage of the ITIH4 variants ITIH4 WT, ITIH4 S282A, ITIH4 S284A, ITIH4 T350A, and ITIH4 S282A + S284A + T350A was performed by mixing MASP-1 EK (final concentration of 2.5 μg/ml) with ITIH4-containing culture supernatant (final ITIH4 concentration of 25 μg/ml) in TBS, 2 mM $CaCl_2$, and 0.1% (v/v) sodium azide. The samples were incubated at 37°C; time points were stopped with SDS-PAGE loading buffer, and anti-ITIH4 WBs were performed. Band intensities were quantified by densitometry.

Cleavage of ITIH4 by MBL–MASP-1 complexes bound on a surface

Recombinant MBL was bound to mannose-derivatized TOYOPEARL HW-75F resin (Sigma-Aldrich) by incubating 0.25 μg of MBL per μl of resin in TBST and 5 mM $CaCl_2$ for 2 hours at room temperature (RT). The beads were washed thrice; MASP-1 EK or MASP-1 EK S646A were added (25 ng of MASP-1 EK per μl of resin), and the samples were incubated overnight at 4°C. A negative control was included that did not receive MBL but did receive MASP-1 EK. The resin was washed thrice, and ITIH4 was added to the sample (375 ng of ITIH4 per μl of resin). The samples were incubated at 37°C, and the reaction was stopped at different time points by mixing aliquots with SDS-PAGE loading buffer. Cleavage of ITIH4 was monitored by SDS-PAGE and Coomassie staining, as described above.

Immunoassay for detection of ITIH4–MASP-1 complexes

Microtiter wells were incubated with 100 μl of anti-ITIH4 (5 μg/ml) or with 100 μl of anti–MASP-1/3 antibody (5 μg/ml). Subsequently, the wells were blocked with HSA. To form complexes between ITIH4 and MASP-1, serum was diluted to 10% in TBST/Ca^{2+} together with MASP-1cf (0 to 20 μg/ml). The samples were incubated at RT for 1.5 hours and diluted fivefold in TBST/Ca^{2+}. Then, 100 μl of sample was added to the plate in duplicates and incubated for 1.5 hours at RT. To detect complexes, the wells were washed in TBST/Ca^{2+} and biotinylated anti–MASP-1/3 (1 μg/ml) was added to anti–ITIH4–coated wells, whereas biotinylated, affinity-purified anti-ITIH4 (1 μg/ml) was added to anti–MASP-1/3–coated wells. The samples were incubated for 1.5 hours at RT, the wells were washed thrice in TBST/Ca^{2+} and received Eu^{3+}-labeled streptavidin (0.1 μg/ml; PerkinElmer) diluted in TBST and 25 μM EDTA. The wells were incubated for 1 hour at RT, washed thrice in TBST/Ca^{2+}, and incubated briefly with 200 μl of enhancement solution (Ampliqon A/S) before measuring the fluorescence by time-resolved fluorometry using a VICTOR X5 plate reader (PerkinElmer). The dose dependency of the assay on ITIH4 was monitored by keeping the concentration of MASP-1cf at 5 μg/ml and varying the concentration of recombinant ITIH4 between 0 and 500 μg/ml. To verify the specificity of the assays, the samples were added in parallel to wells coated with isotype control antibodies. For the anti–MASP-1/3 antibody, the isotype control was mouse IgG (7404304; Lampire), while rabbit IgG (7406404; Lampire) was used as a control for anti–ITIH4–coated wells.

Varying concentrations (0.22 to 450 nM) of the different MASP-1 variants (see Fig. 2D) were added to NHS to assess their ability to form complexes with ITIH4. The assay was performed using anti–ITIH4–coated wells, as described above, with minor modifications. To increase the signal-to-noise ratio, the serum concentration during complex formation was 20%, and biotinylated anti–MASP-1 antibody was used for detection.

To outline the elution profiles of ITIH4–MASP-1 complexes by SEC, serum was mixed with MASP-1cf, MASP-1cf S646A, or MASP-1 SP in TBS to yield a final serum concentration of 75% and a final MASP-1 concentration of 440 nM. These samples were incubated for 1.5 hours at RT, centrifuged at 10,000*g* for 10 min, and fractionated on a Superose 6 Increase 10/300 GL column (GE Healthcare Life Sciences) equilibrated in TBS. Fractions from serum that received MASP-1cf or MASP-1cf S646A were diluted sixfold in TBST/Ca^{2+} and measured in the ITIH4–MASP-1 complex assays to determine the elution profile of the complexes. Similarly, to locate ITIH4–MASP-1 SP complexes, the fractions were diluted twofold in TBST/Ca^{2+} and added to anti–ITIH4–coated wells, followed by detection using biotinylated anti–MASP-1. The elution profile of total ITIH4 was defined by diluting the fractions 500-fold and using the polyclonal rabbit anti-ITIH4 antibody for capture and detection.

To investigate the importance of divalent cations, normal human serum was dialyzed thrice against TBS and 10 mM EDTA, followed by three dialysis steps against TBS to remove EDTA. Dialyzed serum or nondialyzed serum were diluted to 10% in TBS together with

MASP-1 EK (final concentration of 3 μg/ml) and divalent cations (final concentration of 5 mM; $CaCl_2$, $MgCl_2$, $CuCl_2$, $ZnCl_2$, $NiCl_2$, and $MnCl_2$). Complex formation and detection of complexes were performed as described above using anti–MASP-1/3–coated wells and biotinylated anti-ITIH4 for detection.

Complex formation between MASP-1 EK and ITIH4 variants in human embryonic kidney 293-F culture supernatant was performed by incubating MASP-1 EK (3 μg/ml) or MASP-1 EK S646A (3 μg/ml) with supernatant containing varying concentrations (0 to 100 μg/ml) of ITIH4 WT, ITIH4 S282A, ITIH4 S284A, ITIH4 T350A, or ITIH4 S282A + S284A + T350A. Complex formation and detection using anti–MASP-1/3–coated wells were performed as described above for serum, with the exception that the fivefold dilution was made using 20 mM tris, 1 M NaCl, 2 mM $CaCl_2$, 1 mM $MgCl_2$, 0.05% Tween 20, HSA (1 mg/ml), and mouse IgG (100 μg/ml) (pH 7.4).

To assess the influence of high salt and EDTA on the ITIH4–MASP-1cf complexes, an additional step was included in the assay. Upon capture of the complexes by the coating antibody, the wells were incubated in different buffers for 1 hour at RT. These buffers were either 25 mM tris, 0.05% Tween 20, and 5 mM $CaCl_2$ (pH 7.4) with varying concentrations of NaCl (145, 250, 500, 750, or 1000 mM) or 25 mM tris, 145 mM NaCl, 0.05% Tween 20, and 10 mM EDTA (pH 7.4). After this incubation step, the wells were washed in TBST and 5 mM $CaCl_2$, and the rest of the assay was performed as described above. The data were normalized by defining the signal from the sample in 145 mM NaCl as 100% complex formation.

H. alvei–induced formation of ITIH4–MASP-1 complexes in human serum

The *H. alvei* strain polish collection of microorganisms (PMC) 1200 was cultured as previously described (*23*) and fixated by adding formaldehyde to 1% (v/v). The bacteria were equilibrated in TBST, 2 mM $CaCl_2$, and 1 mM $MgCl_2$ and mixed with serum to yield final *H. alvei* concentrations ranging from 0.25×10^9 to 1.5×10^9 bacteria/ml in 12.5% serum. The total volume was 250 μl. As controls, the MASP-1 inhibitor SGMI-1 was added to a final concentration of 5 μM, or the sample was prepared in TBST and 10 mM EDTA. Moreover, serum from an H-ficolin–deficient donor was used instead of normal human serum. The samples were incubated at 37°C for 2 hours on a rotor; the bacteria were pelleted by centrifugation and washed thrice in TBST, and H-ficolin–MASP complexes were eluted from *H. alvei* using 225 μl of 25 mM tris, 1 M NaCl, and 10 mM EDTA (pH 7.4). The eluates were added in duplicates to anti–MASP-1/3–coated wells, and complexes were quantified using biotinylated, affinity-purified anti-ITIH4, as described above. Wells that only received elution buffer was used to define the background signal.

ITIH4-protease complex formation detected by SEC

Generation of ITIH4–MASP-1cf complexes using purified proteins was conducted by incubating 11 μM ITIH4 (1103 μg/ml) with 4.4 μM MASP-1cf (200 μg/ml) in different buffers at 37°C for 1 hour. These buffers were TBS and 2 mM $CaCl_2$ (Ca^{2+}); TBS, 2 mM $CaCl_2$, and 1 mM $MgCl_2$ (Ca^{2+}/Mg^{2+}); or TBS, 2 mM $CaCl_2$, and 1 mM $NiCl_2$ (Ca^{2+}/Ni^{2+}). After incubation, the SP inhibitor Pefabloc was added to 2.0 mM to quench MASP-1 activity. Furthermore, buffer was added to the sample (0.2 times the sample volume), which enabled us to vary the buffer composition between the cleavage step and SEC fractionation. The buffers added after cleavage either yielded TBS and 2 mM $CaCl_2$; TBS, 2 mM $CaCl_2$, and 1 mM $MgCl_2$; or TBS and 10 mM EDTA (EDTA). During SEC fractionation, the Superdex 200 Increase GL 30/100 column (GE Healthcare Life Sciences) was equilibrated in these buffers or Ca^{2+}/Ni^{2+}. A total of 200 μl of sample was loaded on the column for SEC analysis. To examine the content of the different peaks, SEC fractions were analyzed by SDS-PAGE, followed by silver staining.

In general, complex formation using MASP-2cf was performed as described for MASP-1cf. However, the concentrations of MASP-2cf and ITIH4 were 4 and 6 μM, respectively. To compare complex formation for MASP-1cf and MASP-2cf, an experiment with MASP-1cf was also performed using these concentrations. To investigate complex formation between ITIH4 and MASP-1 EK, ITIH4 (6.25 μM) and MASP-1 EK (2.5 μM) were incubated in Ca^{2+} or Ca^{2+}/Mg^{2+}. A Superose 6 Increase 10/300 GL column (GE Healthcare Life Sciences) was equilibrated in the same buffer as used for complex formation, and the sample was fractionated by SEC to detect complex formation. Kallikrein-ITIH4 complexes were formed by incubating ITIH4 (13.6 μM) with plasma kallikrein (3.47 μM; Sigma-Aldrich, no. K2638) at 37°C for 15 min in Ca^{2+} or Ca^{2+}/Mg^{2+}. Following complex formation, Pefabloc-containing buffer was added (0.3 times the sample volume) to yield 2 mM Pefabloc, and 100 μl was injected onto a Superdex 200 Increase GL 30/100 column. To identify kallikrein-containing fractions, SEC fractions were analyzed by anti-kallikrein WB using a rabbit anti-kallikrein antibody (Abcam, no. ab44392).

Analysis of ITIH4-mediated protease inhibition

To form ITIH4–MASP-1cf complexes, ITIH4 (17.6 μM) was incubated with MASP-1cf (4.4 μM) for 1 hour at 37°C in Ca^{2+}/Mg^{2+} and purified by SEC, as described above. The complex-containing fractions were pooled and concentrated, and the MASP-1 concentration in the sample was determined by an immunoassay (*12*). The activity against the tripeptide substrate FGR-AMC (methylsulfonyl-D-Phe-Gly-Arg-AMC; American Diagnostica) was measured by mixing dilutions of ITIH4–MASP-1cf or free MASP-1cf with FGR-AMC (final concentration of 0.1 mM) in microtiter wells and incubating the plate at 37°C. Cleavage was followed at various time points (fig. S8) by measuring fluorescence at 460 nm after excitation at 355 nm. To determine the initial rates of cleavage, the data series were truncated to enable linear regression that fitted with $R^2 > 0.98$ using Prism version 6 (GraphPad software). The cleavage of C2 S679A was followed by mixing C2 (final concentration of 640 μg/ml) with free MASP-1cf or ITIH4–MASP-1cf with a final MASP-1 concentration of 4.55 μg/ml in Ca^{2+}/Mg^{2+}. The samples were incubated at 37°C, and aliquots were withdrawn at different time points and stopped by mixing with SDS-PAGE loading buffer. The samples were analyzed by SDS-PAGE, followed by Coomassie staining, and cleavage of C2 was quantified by measuring the band intensities using densitometry.

The effect of ITIH4 on MASP–2cf–mediated cleavage of FGR-AMC was measured by incubating MASP-2cf (1.5 μM) with ITIH4 (18 μM) in Ca^{2+} or Ca^{2+}/Mg^{2+}. Moreover, a control was made with MASP-2cf Ca^{2+}/Mg^{2+} without addition of ITIH4. These samples were incubated at 37°C for 45 min before they were placed on ice. Two sets of dilution series were made using these samples. One was mixed with FGR-AMC, and cleavage was measured, as described for MASP-1cf. The other dilution series (ranging from 0 to 150 pM MASP-2cf) were added to anti–MASP-2–coated microtiter wells, incubated for 2 hours at 4°C, and the wells were washed thrice in Ca^{2+} or Ca^{2+}/Mg^{2+}. Purified C4 (2.0 μg/ml) in $MgCl_2$ Ca^{2+}/Mg^{2+} was added to the wells; the plates were incubated at 37°C for 2 hours and washed

thrice in TBST, and C4 deposition was estimated using biotinylated rabbit anti-C4c (no. Q0369, Dako). Eu^{3+}-labeled streptavidin was added, and deposition was measured using time-resolved fluorometry, as described above. For each plate, the highest signal was defined as 100% C4 deposition.

To directly follow the ITIH4-mediated inhibition of C2 and C4 cleavage by MASP-2cf temporally, MASP-2cf (0.23 μM) was incubated with ITIH4 (18 μM) in Ca^{2+} or Ca^{2+}/Mg^{2+} for 1 hour at 37°C. The samples were diluted 9.2-fold in Ca^{2+} or Ca^{2+}/Mg^{2+} before mixing it with the substrate of interest to yield 2.7 nM MASP-2cf, 211 nM ITIH4, 1850 nM C2 S679A, or 787 nM C4. Cleavage was examined by incubating the samples at 37°C and quenching the reaction by adding SDS-PAGE loading buffer at the various time points. Analysis of C2 cleavage was performed using nonreduced SDS-PAGE, whereas reducing conditions were used to monitor C4 cleavage. The reactions were quantified using densitometry, and the band intensity at $t = 0$ was defined as 100%. A similar setup was used to investigate the effect of increasing ITIH4 concentrations on MASP-2cf activity. For these experiments, a 1.5-fold dilution series of ITIH4 was prepared in Ca^{2+}/Mg^{2+}, and the samples were mixed with MASP-2cf (0.23 μM) to yield ITIH4 concentrations starting at 15 μM. Complex formation and substrate cleavage were performed as described above, using 15 or 60 min of incubation at 37°C for C4 and C2, respectively. Inhibition of kallikrein-mediated cleavage of HMWK (Sigma-Aldrich, no. 422686) was analyzed by mixing kallikrein (0.02 μM) with varying concentrations of ITIH4 (2.39 μM and twofold dilutions hereof) in Ca^{2+} or Ca^{2+}/Mg^{2+}. Samples were incubated at 37°C for 1 hour before addition of HMWK, yielding 0.018 μM kallikrein, 1.92 μM HMWK, and up to 2.14 μM ITIH4. The cleavage was performed for 2 hours at 37°C.

Complement activity assays

The assay for MBL-mediated LP activity was performed in mannan-coated wells, as previously described (*38*). Serum was diluted to 1% in 4 mM barbital, 145 mM NaCl, 2 mM $CaCl_2$, and 1 mM $MgCl_2$ (pH 7.5) together with different additives: recombinant ITIH4 WT, ITIH4 S282A, ITIH4 S282A + S284A + T350A, C1inh (Sigma-Aldrich), and HSA (CSL Behring, no. 109697). All additives were used in final concentrations that varied from 0 to 4000 nM. Samples were added to the microtiter wells, which were incubated at 37°C for 1.5 hours. Deposited C3 fragments were detected using biotinylated rabbit anti-C3d (no. A0063, Dako), while C4 fragment deposition was quantified using biotinylated rabbit anti-C4c (no. Q0369, Dako). Eu^{3+}-labeled streptavidin was added, and deposition was measured using time-resolved fluorometry, as described above. Furthermore, the effect of ITIH4 WT and HSA on MBL and MASP binding was examined using either biotinylated anti-MBL (0.1 μg/ml) or biotinylated anti–MASP-1/3 (1.0 μg/ml), respectively. In these experiments, serum from an MBL-deficient donor was included as a negative control. MBL-driven LP activity in murine serum was tested in mannan-coated wells, as described above with minor modifications. The assays were performed using 0.2% serum from male C57BL/6 mice, and LP activity was detected at the level of C4 fragment deposition using a rat anti-mouse C4 antibody (Connex GmbH, no. RMC16D2), followed by a biotinylated rabbit anti-rat IgG antibody (Dako, no. E0468) and Eu^{3+}-labeled streptavidin. Similarly, LP activity driven by H-ficolin in human serum was examined using acetylated BSA (Sigma-Aldrich) as the solid-phase ligand. Each well was coated with 1 μg of acetylated BSA, and the assay was performed as described for the mannan-based LP assay using ITIH4 WT, C1inh, and HSA.

Complement activity by the CP was investigated by coating microtiter wells with 100 μl of human IgG (10 μg/ml; CSL Behring, no. 007815). The assay was performed as described for the LP assays with a serum concentration of 0.5% using ITIH4 WT, C1inh, and HSA as additives. An inhibitory nanobody that binds to C3 (C3Nb) and prevents its cleavage was included as a control. The assay for AP activity was performed in zymosan-coated wells, as previously described (*15*). This was performed in a buffer that prevents activation of the LP and CP. The assay was carried out in 16.67% serum, and the effect of HSA, ITIH4, and C3Nb on the C3 fragment deposition was tested in concentrations from 0 to 4000 nM.

For all assays, the data were normalized by defining 100% deposition (of either C3 or C4 fragments) as the signal from serum without any additives. IC_{50} values were estimated using the "log(inhibitor) vs. normalized response – variable slope" in Prism version 6 (GraphPad software). All data were fitted with $R^2 > 0.75$.

Statistical analysis

All data except gels and WBs were represented and analyzed using Prism version 6 (GraphPad software). Densitometry analyses were performed using the Fiji software (*39*). Data points are presented as mean values, and error bars represent SDs. Statistical tests are detailed in the respective figure legends and were performed using Prism version 6 (GraphPad software).

SUPPLEMENTARY MATERIALS

Supplementary material for this article is available at http://advances.sciencemag.org/cgi/content/full/7/2/eaba7381/DC1

View/request a protocol for this paper from *Bio-protocol*.

REFERENCES AND NOTES

1. L. Zhuo, K. Kimata, Structure and function of inter-α-trypsin inhibitor heavy chains. *Connect. Tissue Res.* **49**, 311–320 (2008).
2. L. Zhuo, V. C. Hascall, K. Kimata, Inter-α-trypsin inhibitor, a covalent protein-glycosaminoglycan-protein complex. *J. Biol. Chem.* **279**, 38079–38082 (2004).
3. J. Potempa, K. Kwon, R. Chawla, J. Travis, Inter-α-trypsin inhibitor. Inhibition spectrum of native and derived forms. *J. Biol. Chem.* **264**, 15109–15114 (1989).
4. E. Soury, E. Olivier, M. Daveau, M. Hiron, S. Claeyssens, J. L. Risler, J. P. Salier, The H4P heavy chain of inter-α-inhibitor family largely differs in the structure and synthesis of its prolin-rich region from rat to human. *Biochem. Biophys. Res. Commun.* **243**, 522–530 (1998).
5. X. P. Pu, A. Iwamoto, H. Nishimura, S. Nagasawa, Purification and characterization of a novel substrate for plasma kallikrein (PK-120) in human plasma. *Biochim. Biophys. Acta Protein Struct. Mol.* **1208**, 338–343 (1994).
6. Y. Tang, K. Kitisin, W. Jogunoori, C. Li, C.-X. Deng, S. C. Mueller, H. W. Ressom, A. Rashid, A. R. He, J. S. Mendelson, J. M. Jessup, K. Shetty, M. Zasloff, B. Mishra, E. P. Reddy, L. Johnson, L. Mishra, Progenitor/stem cells give rise to liver cancer due to aberrant TGF-β and IL-6 signaling. *Proc. Natl. Acad. Sci. U.S.A.* **105**, 2445–2450 (2008).
7. J. Song, M. Patel, C. N. Rosenzweig, Y. Chan-Li, L. J. Sokoll, E. T. Fung, N.-H. Choi-Miura, M. Goggins, D. W. Chan, Z. Zhang, Quantification of fragments of human serum inter-α-trypsin inhibitor heavy chain 4 by a surface-enhanced laser desorption/ionization-based immunoassay. *Clin. Chem.* **52**, 1045–1053 (2006).
8. H. Tanaka, M. Shimazawa, M. Takata, H. Kaneko, K. Tsuruma, T. Ikeda, H. Warita, M. Aoki, M. Yamada, H. Takahashi, I. Hozumi, H. Minatsu, T. Inuzuka, H. Hara, ITIH4 and Gpx3 are potential biomarkers for amyotrophic lateral sclerosis. *J. Neurol.* **260**, 1782–1797 (2013).
9. M.-S. Kim, B.-H. Gu, S. Song, B.-C. Choi, D.-H. Cha, K.-H. Baek, ITI-H4, as a biomarker in the serum of recurrent pregnancy loss (RPL) patients. *Mol. Biosyst.* **7**, 1430–1440 (2011).
10. J. Wang, X. Zhu, X. Xiong, P. Ge, H. Liu, N. Ren, F. A. Khan, X. Zhou, L. Zhang, X. Yuan, X. Chen, Y. Chen, C. Hu, I. D. Robertson, H. Chen, A. Guo, Identification of potential urine proteins and microRNA biomarkers for the diagnosis of pulmonary tuberculosis patients. *Emerg. Microbes Infect.* **7**, 63 (2018).

11. G. Bajic, S. E. Degn, S. Thiel, G. R. Andersen, Complement activation, regulation, and molecular basis for complement-related diseases. *EMBO J.* **34**, 2735–2757 (2015).
12. A. Troldborg, A. Hansen, S. W. K. Hansen, J. C. Jensenius, K. Stengaard-Pedersen, S. Thiel, Lectin complement pathway proteins in healthy individuals. *Clin. Exp. Immunol.* **188**, 138–147 (2017).
13. D. Héja, A. Kocsis, J. Dobó, K. Szilágyi, R. Szász, P. Závodszky, G. Pál, P. Gál, Revised mechanism of complement lectin-pathway activation revealing the role of serine protease MASP-1 as the exclusive activator of MASP-2. *Proc. Natl. Acad. Sci. U.S.A.* **109**, 10498–10503 (2012).
14. J. Dobó, D. Szakács, G. Oroszlán, E. Kortvely, B. Kiss, E. Boros, R. Szász, P. Závodszky, P. Gál, G. Pál, MASP-3 is the exclusive pro-factor D activator in resting blood: The lectin and the alternative complement pathways are fundamentally linked. *Sci. Rep.* **6**, 31877 (2016).
15. R. Pihl, L. Jensen, A. G. Hansen, I. B. Thøgersen, S. Andres, F. Dagnæs-Hansen, K. Oexle, J. J. Enghild, S. Thiel, Analysis of factor D isoforms in Malpuech–Michels–Mingarelli–Carnevale patients highlights the role of MASP-3 as a maturase in the alternative pathway of complement. *J. Immunol.* **6**, 2158–2170 (2017).
16. T. R. Kjaer, S. Thiel, G. R. Andersen, Toward a structure-based comprehension of the lectin pathway of complement. *Mol. Immunol.* **56**, 413–422 (2013).
17. J. Dobó, V. Schroeder, L. Jenny, L. Cervenak, P. Závodszky, P. Gál, Multiple roles of complement MASP-1 at the interface of innate immune response and coagulation. *Mol. Immunol.* **61**, 69–78 (2014).
18. N. D. Rawlings, D. P. Tolle, A. J. Barrett, Evolutionary families of peptidase inhibitors. *Biochem. J.* **378**, 705–716 (2004).
19. J. A. Huntington, R. J. Read, R. W. Carrel, Structure of a serpin–protease complex shows inhibition by deformation. *Nature* **407**, 923–926 (2000).
20. K. Paréj, J. Dobó, P. Závodszky, P. Gál, The control of the complement lectin pathway activation revisited: Both C1-inhibitor and antithrombin are likely physiological inhibitors, While α_2-macroglobulin is not. *Mol. Immunol.* **54**, 415–422 (2013).
21. L. Sottrup-Jensen, O. Sand, L. Kristensen, G. H. Fey, The α-macroglobulin bait region. Sequence diversity and localization of cleavage sites for proteinases in five mammalian α-macroglobulins. *J. Biol. Chem.* **264**, 15781–15789 (1989).
22. S. V. Petersen, S. Thiel, L. Jensen, T. Vorup-Jensen, C. Koch, J. C. Jensenius, Control of the classical and the MBL pathway of complement activation. *Mol. Immunol.* **37**, 803–811 (2001).
23. M. Michalski, A. S. Swierzko, J. Lukasiewicz, A. Man-Kupisinska, I. Karwaciak, P. Przygodzka, M. Cedzynski, Ficolin-3 activity towards the opportunistic pathogen, *Hafnia alvei*. *Immunobiology* **220**, 117–123 (2015).
24. C. A. Whittaker, R. O. Hynes, Distribution and evolution of von willebrand/integrin a domains: Widely dispersed domains with roles in cell adhesion and elsewhere. *Mol. Biol. Cell* **13**, 3369–3387 (2002).
25. D. C. Briggs, A. W. W. Langford-Smith, H. L. Birchenough, T. A. Jowitt, C. M. Kielty, J. J. Enghild, X. Clair Baldock, C. M. Milner, A. J. Day, Inter-α-inhibitor heavy chain-1 has an integrin-like 3D structure mediating immune regulatory activities and matrix stabilization during ovulation. *J. Biol. Chem.* **295**, 5278–5291 (2020).
26. J. Björkqvist, A. Jämsä, T. Renné, Plasma kallikrein: The bradykinin-producing enzyme. *Thromb. Haemost.* **110**, 399–407 (2013).
27. M. Okroj, E. Holmquist, J. Sjölander, L. Corrales, T. Saxne, H.-G. Wisniewski, A. M. Blom, Heavy chains of inter alpha inhibitor (Iαl) inhibit the human complement system at early stages of the cascade. *J. Biol. Chem.* **287**, 20100–20110 (2012).
28. H. Kozarcanin, C. Lood, L. Munthe-Fog, K. Sandholm, O. A. Hamad, A. A. Bengtsson, M.-O. Skjoedt, M. Huber-Lang, P. Garred, K. N. Ekdahl, B. Nilsson, The lectin complement pathway serine proteases (MASPs) represent a possible crossroad between the coagulation and complement systems in thromboinflammation. *J. Thromb. Haemost.* **14**, 531–545 (2016).
29. M. A. Bartlomiejczyk, A. S. Swierzko, A. Brzostek, J. Dziadek, M. Cedzynski, Interaction of lectin pathway of complement-activating pattern recognition molecules with Mycobacteria. *Clin. Exp. Immunol.* **178**, 310–319 (2014).
30. L. Scarchilli, A. Camaioni, B. Bottazzi, V. Negri, A. Doni, L. Deban, A. Bastone, G. Salvatori, A. Mantovani, G. Siracusa, A. Salustri, PTX3 interacts with inter-α-trypsin inhibitor: Implications for hyaluronan organization and cumulus oophorus expansion. *J. Biol. Chem.* **282**, 30161–30170 (2007).
31. J. T. B. Crawley, R. de Groot, Y. Xiang, B. M. Luken, D. A. Lane, Unraveling the scissile bond: How ADAMTS13 recognizes and cleaves von Willebrand factor. *Blood* **118**, 3212–3221 (2011).
32. M. W. MacArthur, J. M. Thornton, Influence of proline residues on protein conformation. *J. Mol. Biol.* **218**, 397–412 (1991).
33. C. Gialeli, A. D. Theocharis, N. K. Karamanos, Roles of matrix metalloproteinases in cancer progression and their pharmacological targeting. *FEBS J.* **278**, 16–27 (2011).
34. C. J. Farady, C. S. Craik, Mechanisms of macromolecular protease inhibitors. *Chembiochem* **11**, 2341–2346 (2010).
35. M. S. Brower, P. C. Harpel, Proteolytic cleavage and inactivation of α_2-plasmin inhibitor and CT inactivator by human polymorphonuclear leukocyte elastase. *J. Biol. Chem.* **257**, 9849–9854 (1982).
36. S. J. Kolodziej, T. Wagenknecht, D. K. Strickland, J. K. Stoops, The three-dimensional structure of the human α_2-macroglobulin dimer reveals its structural organization in the tetrameric native and chymotrypsin α_2-macroglobulin complexes. *J. Biol. Chem.* **277**, 28031–28037 (2002).
37. J. Dobó, V. Harmat, L. Beinrohr, E. Sebestyén, P. Závodszky, P. Gál, MASP-1, a promiscuous complement protease: Structure of its catalytic region reveals the basis of its broad specificity. *J. Immunol.* **183**, 1207–1214 (2009).
38. R. K. Jensen, R. Pihl, T. A. F. Gadeberg, J. K. Jensen, K. R. Andersen, S. Thiel, N. S. Laursen, G. R. Andersen, A potent complement factor C3–specific nanobody inhibiting multiple functions in the alternative pathway of human and murine complement. *J. Biol. Chem.* **293**, 6269–6281 (2018).
39. J. Schindelin, I. Arganda-Carreras, E. Frise, V. Kaynig, M. Longair, T. Pietzsch, S. Preibisch, C. Rueden, S. Saalfeld, B. Schmid, J.-Y. Tinevez, D. J. White, V. Hartenstein, K. Eliceiri, P. Tomancak, A. Cardona, Fiji: An open-source platform for biological-image analysis. *Nat. Methods* **9**, 676–682 (2012).
40. S. E. Degn, L. Jensen, P. Gál, J. Dobó, S. H. Holmvad, J. C. Jensenius, S. Thiel, Biological variations of MASP-3 and MAp44, two splice products of the *MASP1* gene involved in regulation of the complement system. *J. Immunol. Methods* **361**, 37–50 (2010).
41. M. Møller-Kristensen, J. C. Jensenius, L. Jensen, N. Thielens, V. Rossi, G. Arlaud, S. Thiel, Levels of mannan-binding lectin-associated serine protease-2 in healthy individuals. *J. Immunol. Methods* **282**, 159–167 (2003).
42. S. Thiel, M. Møller-Kristensen, L. Jensen, J. C. Jensenius, Assays for the functional activity of the mannan-binding lectin pathway of complement activation. *Immunobiology* **205**, 446–454 (2002).
43. A. Troldborg, S. Thiel, M. Trendelenburg, J. Friebus-Kardash, J. Nehring, R. Steffensen, S. W. K. Hansen, M. J. Laska, B. Deleuran, J. C. Jensenius, A. Voss, K. Stengaard-Pedersen, The lectin pathway of complement activation in patients with systemic lupus erythematosus. *J. Rheumatol.* **45**, 1136–1144 (2018).
44. G. Ambrus, P. Gál, M. Kojima, K. Szilágyi, J. Balczer, J. Antal, L. Gráf, A. Laich, B. E. Moffatt, W. Schwaeble, R. B. Sim, P. Závodszky, Natural substrates and inhibitors of mannan-binding lectin-associated serine protease-1 and -2: A study on recombinant catalytic fragments. *J. Immunol.* **170**, 1374–1382 (2003).
45. M. Megyeri, V. Harmat, B. Major, Á. Végh, J. Balczer, D. Héja, K. Szilágyi, D. Datz, G. Pál, P. Závodszky, P. Gál, J. Dobó, Quantitative characterization of the activation steps of mannan-binding lectin (MBL)-associated serine proteases (MASPs) points to the central role of MASP-1 in the initiation of the complement lectin pathway. *J. Biol. Chem.* **288**, 8922–8934 (2013).
46. G. Oroszlán, R. Dani, A. Szilágyi, P. Závodszky, S. Thiel, P. Gál, J. Dobó, Extensive basal level activation of complement mannose-binding lectin-associated serine protease-3: Kinetic modeling of lectin pathway activation provides possible mechanism. *Front. Immunol.* **8**, 1821 (2017).
47. L. C. Wijeyewickrema, T. Yongqing, T. P. Tran, P. E. Thompson, J. E. Viljoen, T. H. Coetzer, R. C. Duncan, I. Kass, A. M. Buckle, R. N. Pike, Molecular determinants of the substrate specificity of the complement-initiating protease, C1r. *J. Biol. Chem.* **288**, 15571–15580 (2013).
48. J. C. Jensenius, P. H. Jensen, K. McGuire, J. L. Larsen, S. Thiel, Recombinant mannan-binding lectin (MBL) for therapy. *Biochem. Soc. Trans.* **31**, 763–767 (2003).
49. D. Héja, V. Harmats, K. Fodor, M. Wilmanns, J. Dobó, K. A. Kékesi, P. Závodszky, P. Gál, G. Pál, Monospecific inhibitors show that both mannan-binding lectin-associated serine protease-1 (MASP-1) and -2 are essential for lectin pathway activation and reveal structural plasticity of MASP-2. *J. Biol. Chem.* **287**, 20290–20300 (2012).
50. S. E. Degn, L. Jensen, A. G. Hansen, D. Duman, M. Tekin, J. C. Jensenius, S. Thiel, Mannan-binding lectin-associated serine protease (MASP)-1 is crucial for lectin pathway activation in human serum, whereas neither MASP-1 nor MASP-3 is required for alternative pathway function. *J. Immunol.* **189**, 3957–3969 (2012).
51. O. Erster, M. Liscovitch, *In Vitro Mutagenesis Protocols*, J. Braman, Ed. (Humana Press, ed. 3, 2010), pp. 157–174.
52. D. G. Deutsch, E. T. Mertz, Plasminogen: Purification from human plasma by affinity chromatography. *Science* **170**, 1095–1096 (1970).
53. E. T. Poulsen, N. S. Nielsen, C. Scavenius, E. H. Mogensen, M. W. Risør, K. Runager, M. V. Lukassen, C. B. Rasmussen, G. Christiansen, M. Richner, H. Vorum, J. J. Enghild, The serine protease HtrA1 cleaves misfolded transforming growth factor β–induced protein (TGFBIp) and induces amyloid formation. *J. Biol. Chem.* **294**, 11817–11828 (2019).
54. S. E. Degn, L. Jensen, A. G. Hansen, D. Duman, M. Tekin, J. C. Jensenius, S. Thiel, MASP-1 is crucial for lectin pathway activation in human serum, while neither MASP-1 nor MASP-3 are required for alternative pathway function. *J. Immunol.* **217**, 1218–1219 (2012).
55. C.-B. Chen, R. Wallis, Two mechanisms for mannose-binding protein modulation of the activity of its associated serine proteases. *J. Biol. Chem.* **279**, 26058–26065 (2004).
56. W. Skala, P. Goettig, H. Brandstetter, Do-it-yourself histidine-tagged bovine enterokinase: A handy member of the protein engineer's toolbox. *J. Biotechnol.* **168**, 421–425 (2013).

57. J. Rappsilber, M. Mann, Y. Ishihama, Protocol for micro-purification, enrichment, pre-fractionation and storage of peptides for proteomics using StageTips. *Nat. Protoc.* **2**, 1896–1906 (2007).
58. D. N. Perkins, D. J. Pappin, D. M. Creasy, J. S. Cottrell, Probability-based protein identification by searching sequence databases using mass spectrometry data. *Electrophoresis* **20**, 3551–3567 (1999).
59. P. Matsudaira, Sequence from picomole quantities of proteins electroblotted onto polyvinylidene difluoride membranes. *J. Biol. Chem.* **262**, 10035–10038 (1987).
60. C. E. Blanchet, A. Spilotros, F. Schwemmer, M. A. Graewert, A. Kikhney, C. M. Jeffries, D. Franke, D. Mark, R. Zengerle, F. Cipriani, S. Fiedler, M. Roessle, D. I. Svergun, Versatile sample environments and automation for biological solution x-ray scattering experiments at the P12 beamline (PETRA III, DESY). *J. Appl. Cryst.* **48**, 431–443 (2015).
61. D. Franke, A. G. Kikhney, D. I. Svergun, Automated acquisition and analysis of small angle x-ray scattering data. *Nucl. Instrum. Methods Phys. Res. A* **689**, 52–59 (2012).
62. D. Franke, M. V. Petoukhov, P. V. Konarev, A. Panjkovich, A. Tuukkanen, H. D. T. Mertens, A. G. Kikhney, N. R. Hajizadeh, J. M. Franklin, C. M. Jeffries, D. I. Svergun, *ATSAS 2.8*: A comprehensive data analysis suite for small-angle scattering from macromolecular solutions. *J. Appl. Cryst.* **50**, 1212–1225 (2017).
63. C. Suloway, J. Pulokas, D. Fellmann, A. Cheng, F. Guerra, J. Quispe, S. Stagg, C. S. Potter, B. Carragher, Automated molecular microscopy: The new Leginon system. *J. Struct. Biol.* **151**, 41–60 (2005).
64. T. Grant, A. Rohou, N. Grigorieff, *cis*TEM, user-friendly software for single-particle image processing. *eLife* **7**, e35383 (2018).
65. S. H. W. Scheres, RELION: Implementation of a Bayesian approach to cryo-EM structure determination. *J. Struct. Biol.* **180**, 519–530 (2012).
66. T. R. Kjaer, S. Thiel, *The Complement System: Methods and Protocols*, M. Gadjeva, Ed. (Humana Press, 2014), pp. 131–139.
67. A. Waterhouse, M. Bertoni, S. Bienert, G. Studer, G. Tauriello, R. Gumienny, F. T. Heer, T. A. P. de Beer, C. Rempfer, L. Bordoli, R. Lepore, T. Schwede, SWISS-MODEL: Homology modelling of protein structures and complexes. *Nucleic Acids Res.* **46**, W296–W303 (2018).

Acknowledgments: We thank A. Zarantonello for donating the enterokinase and purified C2. We acknowledge K. Yamamoto for donating MMP-3, MMP-13, ADAMTS-4, and ADAMTS-5 and L. del Amo Maestro for providing ADAMTS-13. Moreover, we are grateful to A. Troldborg for providing the serum from the H-ficolin–deficient donor. We also acknowledge U. B. Skov Sørensen for preparing *H. alvei*. We thank J. Balczer for excellent technical assistance and G. Pál for advice on MASP inhibitors. Last, we acknowledge S. E. Degn for valuable discussions. **Funding:** S.T. was supported by the Independent Research Fund Denmark (DFF; 4183-00450) and CellPAT, a Danish National Research Foundation Center of Excellence (DNRF135). G.R.A. was supported by the Lundbeck Foundation (BRAINSTRUC, R155-2015-2666), the Novo Nordisk Foundation (NNF18OC0052105), and the Carlsberg Foundation (CF18-0067). J.D. and P.G. were supported by the Hungarian National Research, Development and Innovation Office OTKA grants K119374 and KH130376. **Author contributions:** R.P., G.R.A., and S.T. designed the experiments and analyzed the data. R.P., L.J., A.G.H., R.K.J, and E.C.P. conducted the majority of the experimental work, while I.B.T. and J.J.E. performed the mass spectrometry analysis and N-terminal sequencing, and J.D. and P.G. produced the various MASP fragments and SGMI-1. All authors contributed to manuscript preparation. **Competing interests:** The authors declare that they have no competing interests. **Data and materials availability:** All data needed to evaluate the conclusions in the paper are present in the paper and/or the Supplementary Materials. Additional data related to this paper may be requested from the authors.

Submitted 31 December 2019
Accepted 16 November 2020
Published 8 January 2021
10.1126/sciadv.aba7381

Citation: R. Pihl, R. K. Jensen, E. C. Poulsen, L. Jensen, A. G. Hansen, I. B. Thøgersen, J. Dobó, P. Gál, G. R. Andersen, J. J. Enghild, S. Thiel, ITIH4 acts as a protease inhibitor by a novel inhibitory mechanism. *Sci. Adv.* **7**, eaba7381 (2021).